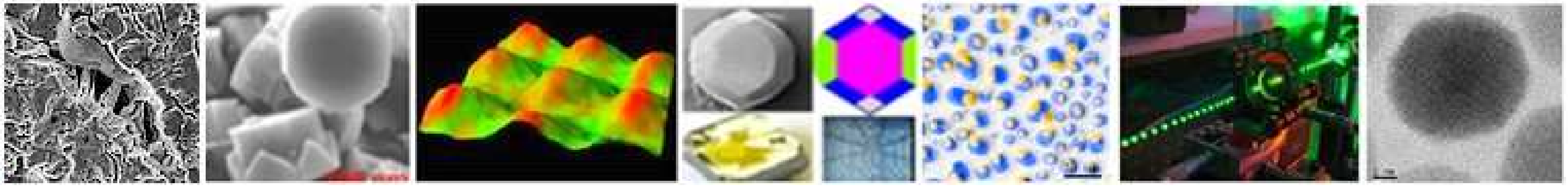

LABEX SEAM

# Compréhension et optimisation des procédés de synthèse de dépôt diamant par plasmas: Contribution de la modélisation et des diagnostics spectroscopiques

G. Lombardi *et al*

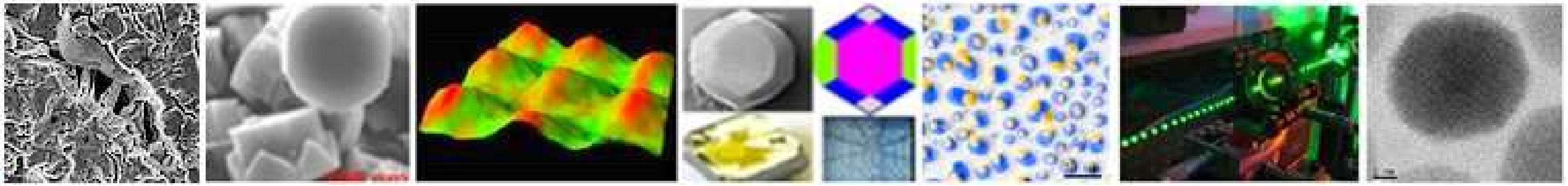

# INTRODUCTION TO

# SYNTHETIC DIAMOND

# Diamond properties

- Exceptional mechanical **Hardness** and **Thermal Conductivity** (2200 W/mK)
- **Wide bangap** semiconductor (5.5 eV)
- **Optical** transparency (Down to 225nm)
- Resistant to **ionizing particles** and chemicals
- **Biocompatible**
- Wide **electrochemical** window

For many applications **only thin diamond layers with moderate quality** (nano or polycrystalline) needed…
However increasing interest in **large size high quality crystals** motivated by high-end applications in optics, electronics, quantum physics… (not just for jewelry!)

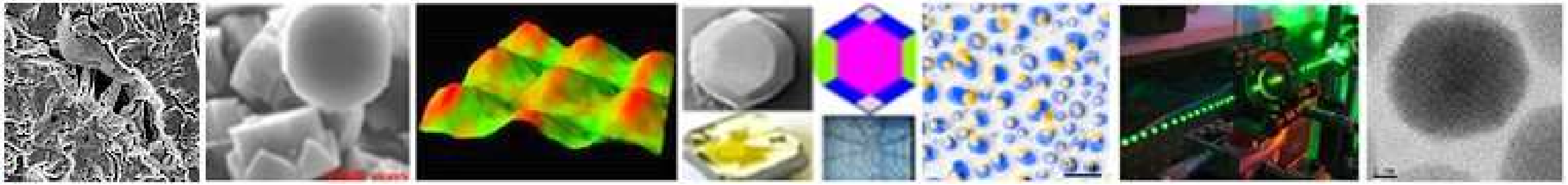

LABEX SEAM

# Single crystal diamond applications


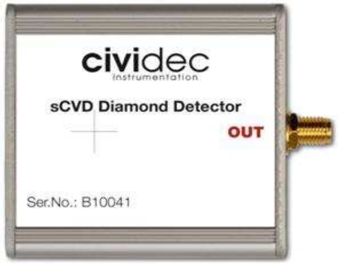


## DIAMOND DETECTORS

For high energy particles
Thick intrinsic layers

## HIGH POWER DEVICES

Thick p+ diamond crystals for vertical diodes

*J. Achard et al. Diam. & Relat. Mat.* ***20, 145-152 (2011).***

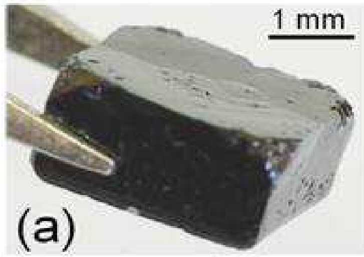


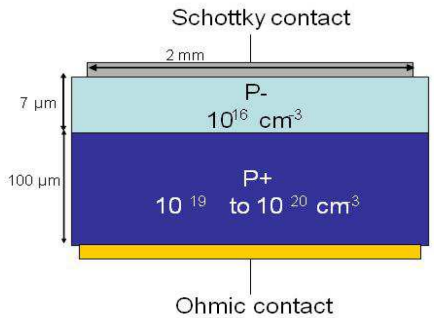


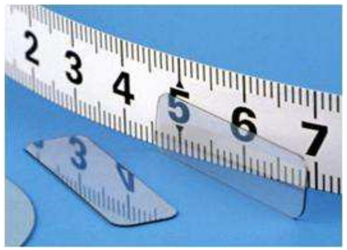

*Diamond Materials*

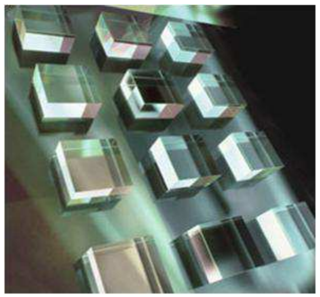

*Element 6*

## OPTICAL WINDOWS

For high-power lasers, gyrotron
and Raman lasers

# Single crystal diamond applications

## LUMINESCENT DEFECTS IN DIAMOND AS QU-BITS FOR MAGNETOMETRY

Gruber et al., *Science* **276**, 2012 (1997)

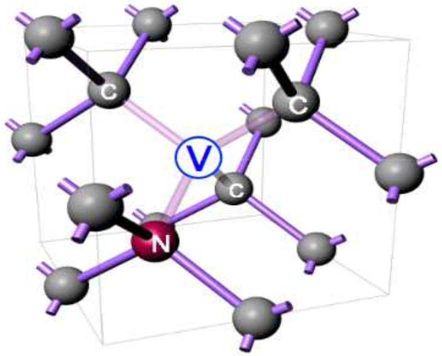


The Nitrogen-Vacancy centre

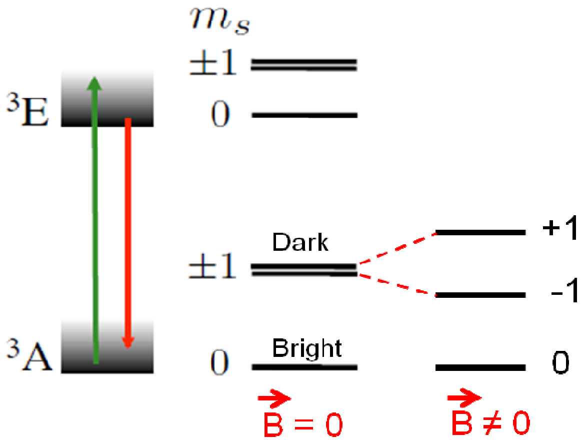


Zeeman splitting of spin states

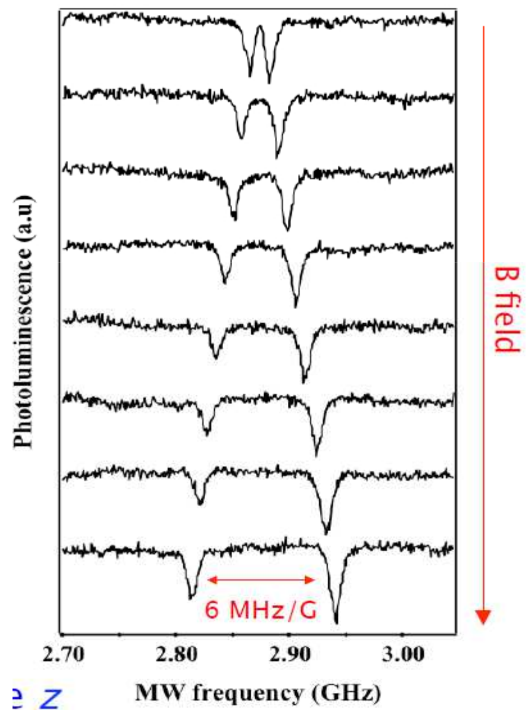


*L. Rondin et al. Magnetometry with nitrogen-vacancy defects in diamond, ArXiv:1311.5214v2 (2013)*

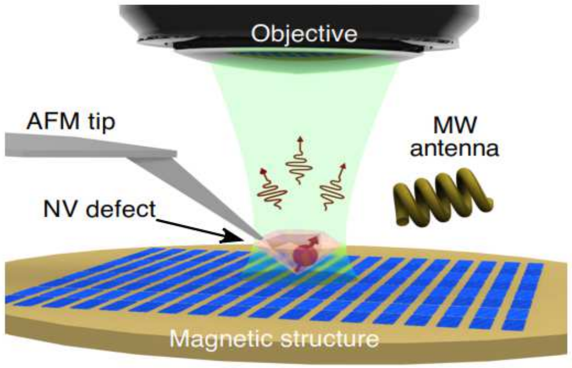


Magnetic field sensing

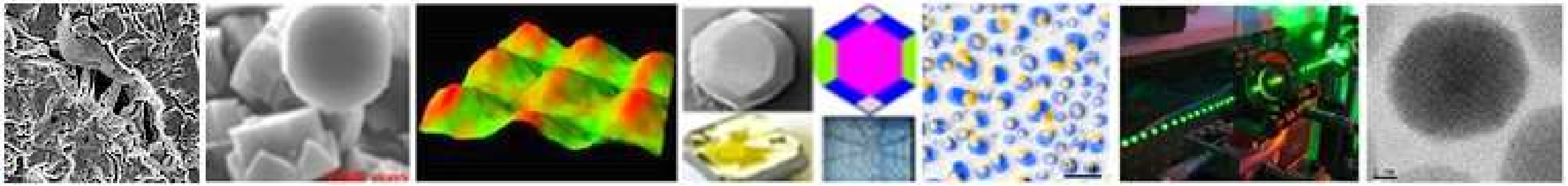

# BASIC PRINCIPLES OF THE PLASMA ASSISTED CHEMICAL VAPOUR DEPOSITION PROCESS

# Plasma-Assisted CVD

## TYPICAL MW-PACVD CONDITIONS

Micro-Wave (600 - 4000 W)

P = 25 - 400 mbar

*Alternative mixtures:*
$H_2/CH_4/B_2H_6$
$Ar/H_2/CH_4$
$H_2/CH_4/CO_2$

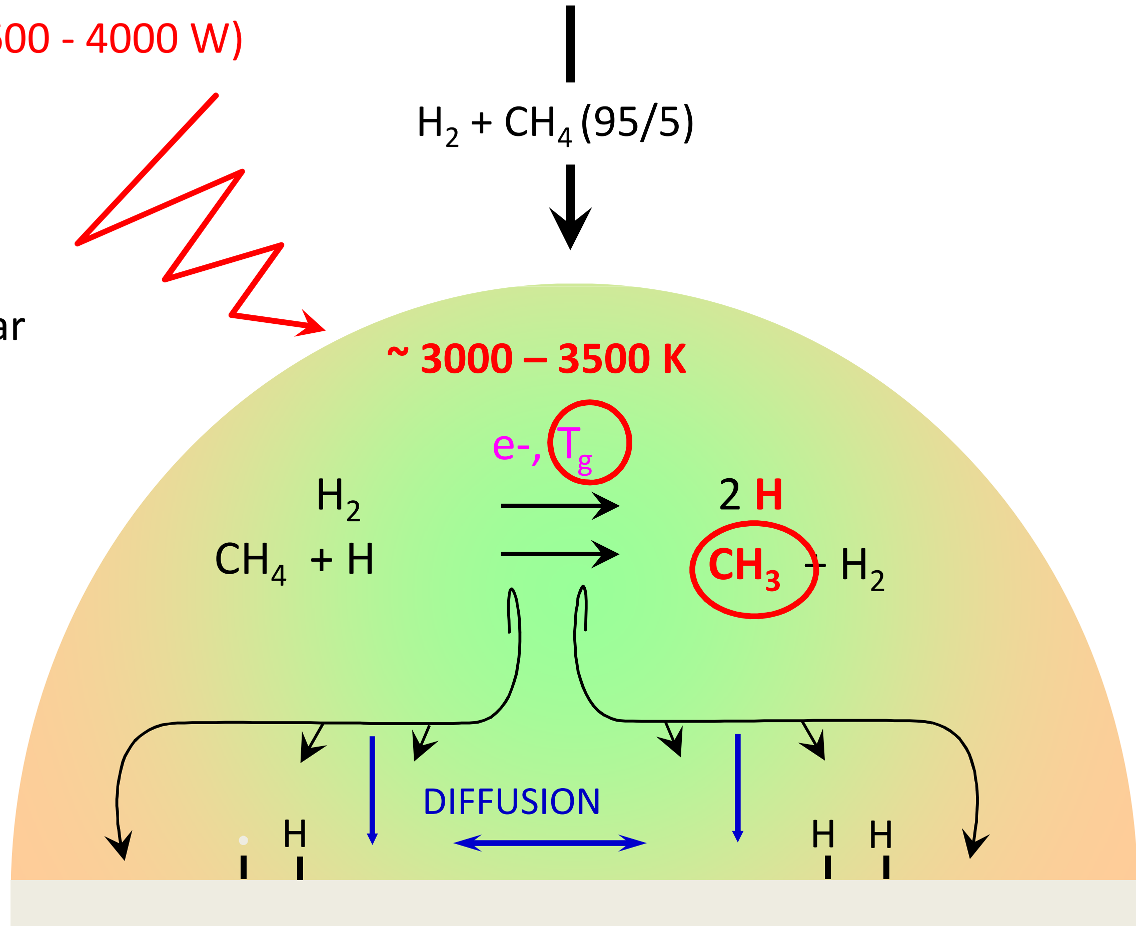


Substrate (Si, HPHT diamond…)

$T_{substrate}$ = 1000 - 1400 K

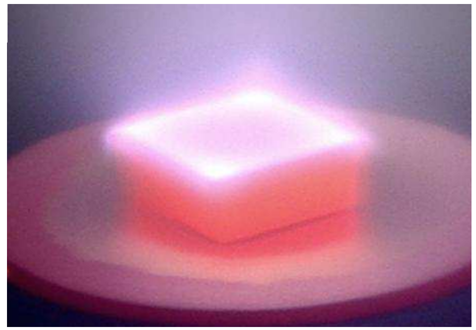

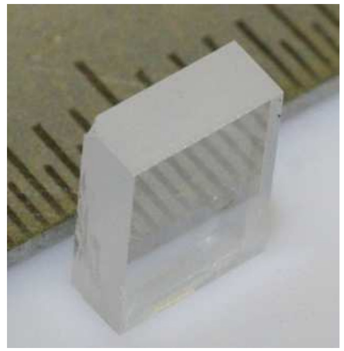

# Mécanismes de croissance

Création de sites actifs

$$Cd-H+H \xrightarrow{k1} Cd^{*}+H_2$$

$$Cd^{*}+H \xrightarrow{k2} Cd-H$$

Adsorption du radical $CH_3$ et deshydrogénation

$$Cd^{*}+CH_3 \underset{k4}{\overset{k3}{\rightleftarrows}} Cd-CH_3$$

$$Cd-CH_3+H \xrightarrow{k5} Cd-CH_2^{*}+H_2$$

$$Cd-CH_2^{*}+H \xrightarrow{k6} Cd-Cd-H+H_2$$

Rôle fondamental de H et $CH_3$

$$\boxed{G_{(100)}=k_3\frac{n_s}{n_d}\left(\frac{k_1}{k_1+k_2}\right)\frac{[CH_3]_s[H]_s}{\frac{k_4}{k_5}+[H]_s}}$$

Quand $[H]_{surface}$ est suffisament élevée ($> 10^{-8}$ mole.cm$^{-3}$) la vitesse de croissance ne dépend que de $[CH_3]_{surface}$

S.J. Harris and D. G. Goodwin (1993), J. Phys. Chem. **97** (1993) 23

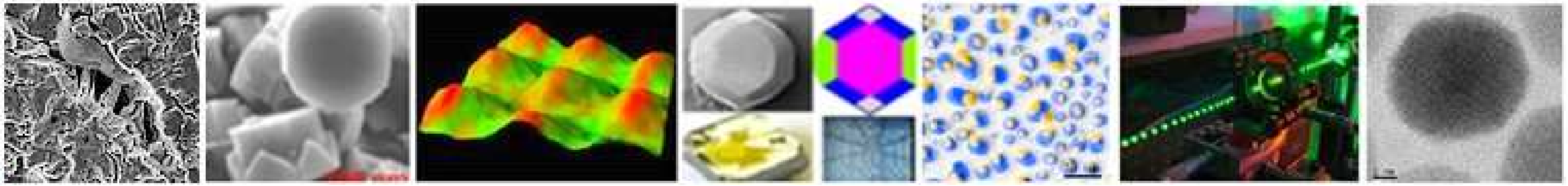

LABEX SEAM

# Plasma-Assisted CVD

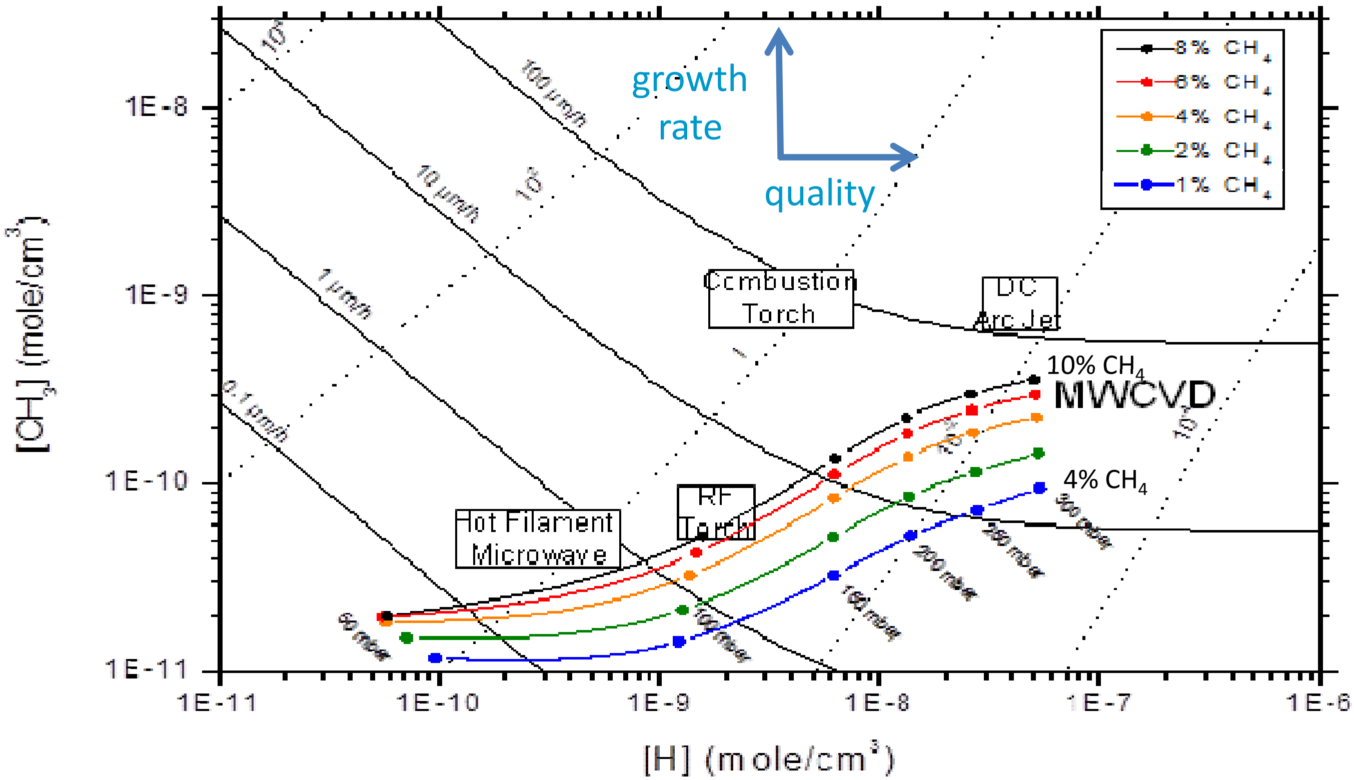


<u>Goodwin's growth model</u>

$$G = \frac{g_1 f^* [C_n H_m][H]}{g_2 + [H]},$$

*Goodwin, D. G. "Scaling laws for diamond chemical-vapor deposition. I. Diamond surface chemistry" J. Appl. Phys. 74 (11) 1993: 6888-6894.*

**Higher pressure and microwave power** → higher gas temperature → easier dissociation of $H_2$ and $CH_4$ → **higher growth rates and higher quality**

F. Silva, K. Hassouni, X. Bonnin et al., Journal of Physics: Condensed Matter **21, 364202 (2009).**

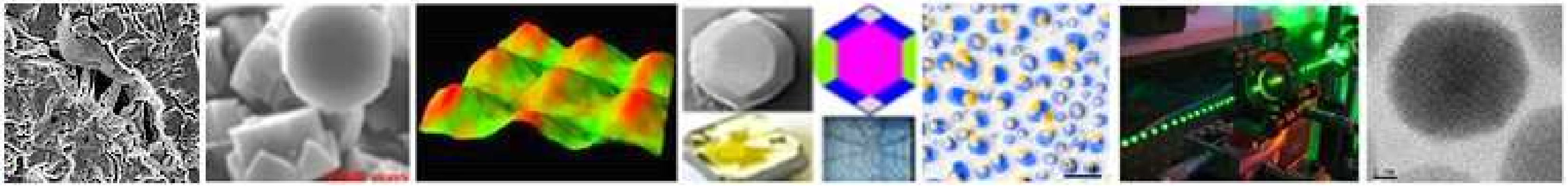

## LABEX SEAM

✓ **Objectives:**

- To better understand the **physico-chemical processes** occurring in Micro-Wave Plasma Assisted Chemical Vapor Deposition (MW-PACVD) reactors
- To **optimize** the MW-PACVD process
- To match the aimed **properties and applications** of **diamond films**

✓ **Approach:**

- As a first step, need of a **thorough analysis of the plasma phase**, to control key parameters of the process : **gas temperature / active species densities**
- **Two example of studies**: (i) mono/micro-crystalline diamond, and (ii) nano-crystalline diamond

✓ **Main tools used:**

- **Advanced plasma diagnostics** (Optical Emission Spectroscopy, IR Laser Absorption Spectroscopy, UV Broadband Absorption Spectroscopy, …)
- **Modelling** (0D and 1D thermochemical fluid models)

✓ **Issues to take into account:**

- **Stiff** temperatures and densities **gradients** (integrated measurements, …)
- **High pressure** (quenching, …)
- **Complex chemistry** of transient species at low concentrations
- …

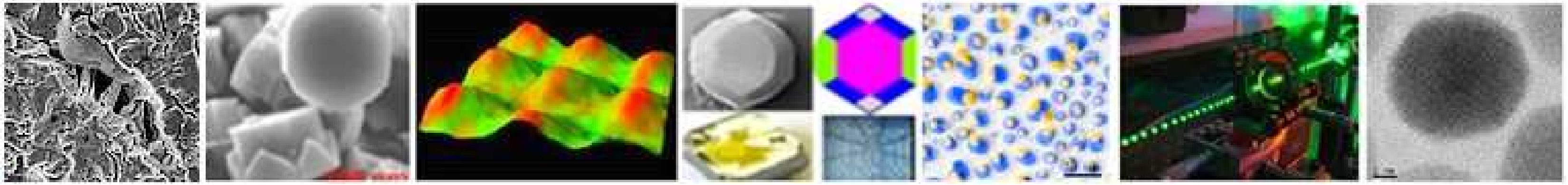

## LABEX SEAM

# Méthodologie

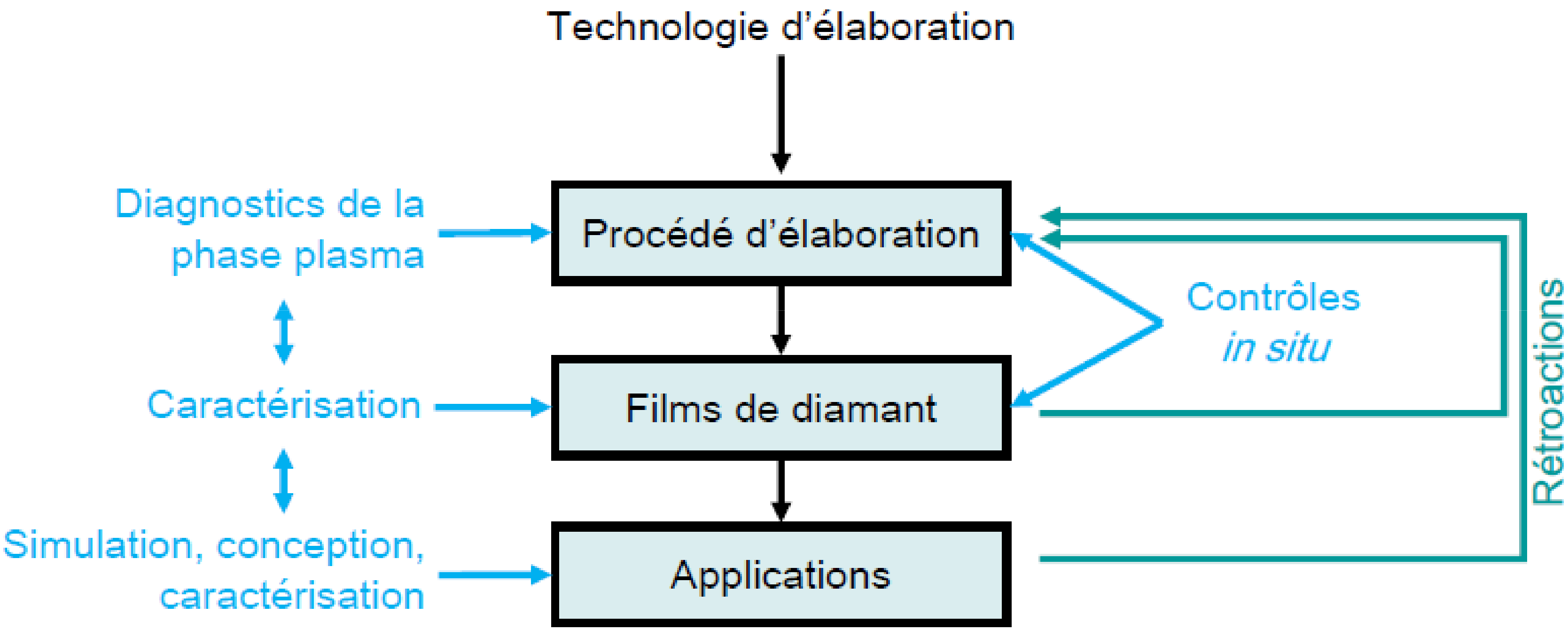


**Procédés – Plasmas - Matériaux - Applications**

# Exemples de réacteurs au LSPM

- Réacteur bell jar

Cavité réelle

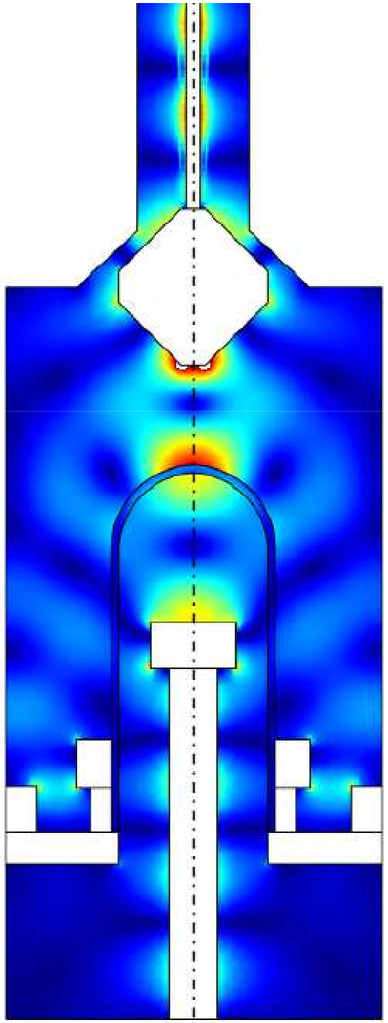

Cavité couplée

- Réacteur métallique

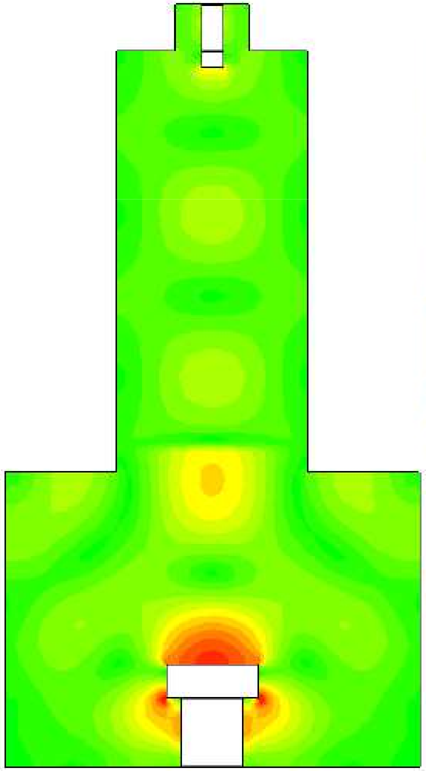

Cavité couplée

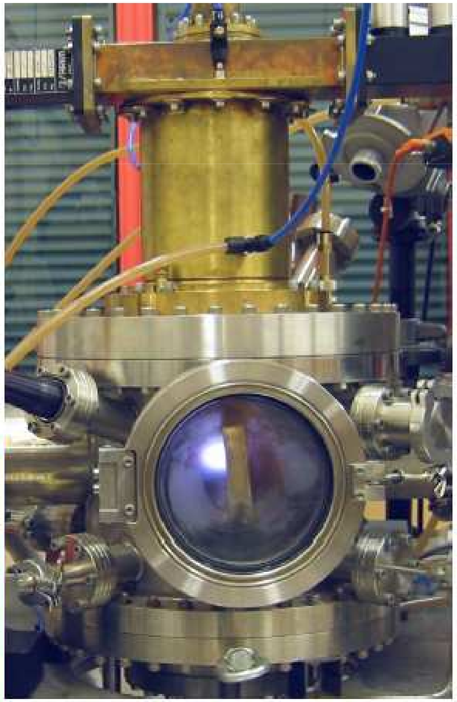

Cavité réelle

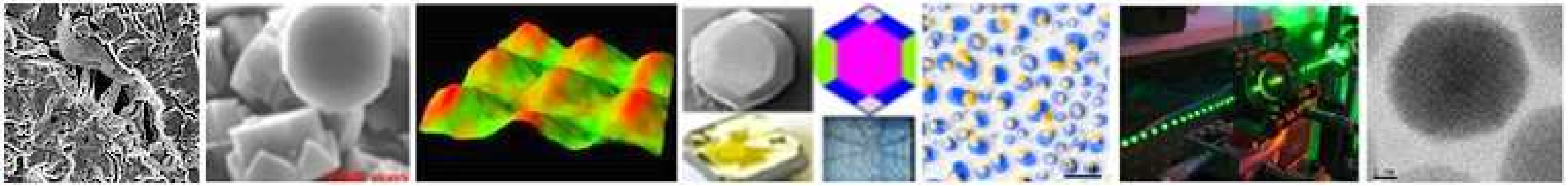

LABEX SEAM

# Outils développés

- **Modèles et codes (Hassouni *et al*)**

| **Modèle 0D** | **Modèle 1D** | **Modèle 2D** |
|---|---|---|
| Modèle plasma $H_2$ pur | Modèle plasma $H_2/CH_4/Ar$ + $\varepsilon$ $B_2H_6$ | Modèle auto-cohérent $H_2$ / $CH_4$ |

**Validation expérimentale (Gicquel *et al*)** : OES, TDLAS, LIF, CARS, Interférométrie MW

| **Réacteur Bell Jar** | **Réacteur métallique** |
|---|---|
| Faibles pressions/ puissances | Fortes pressions/ puissances |
| $T_g$, $T_v$, $T_e$ | $T_g$, $T_e$, $n_e$ |
| H | H |
| Hydrocarbures | Hydrocarbures |

Différence entre basse et haute pression/ puissance : **$e^-$** et **Tg**

# Description des modèles

**Code 1D : Axial et Radial**

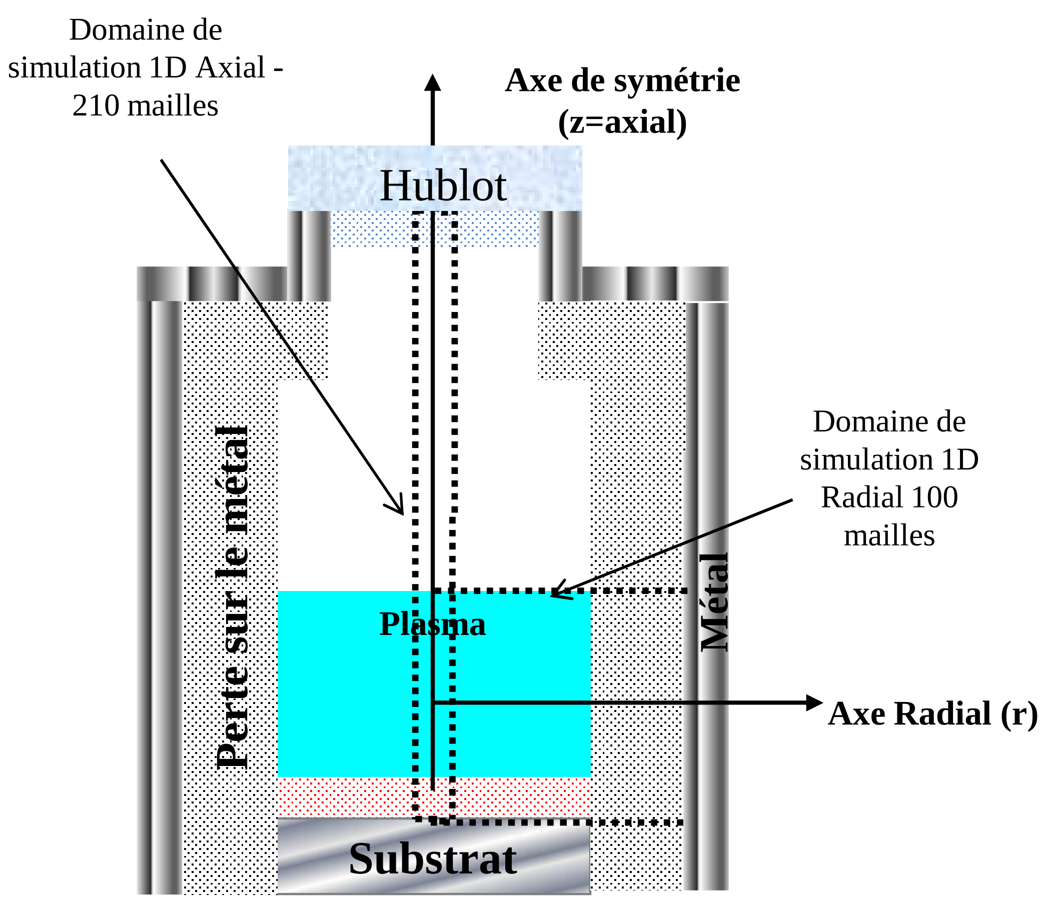


**Modèle 2D axisymétrique**

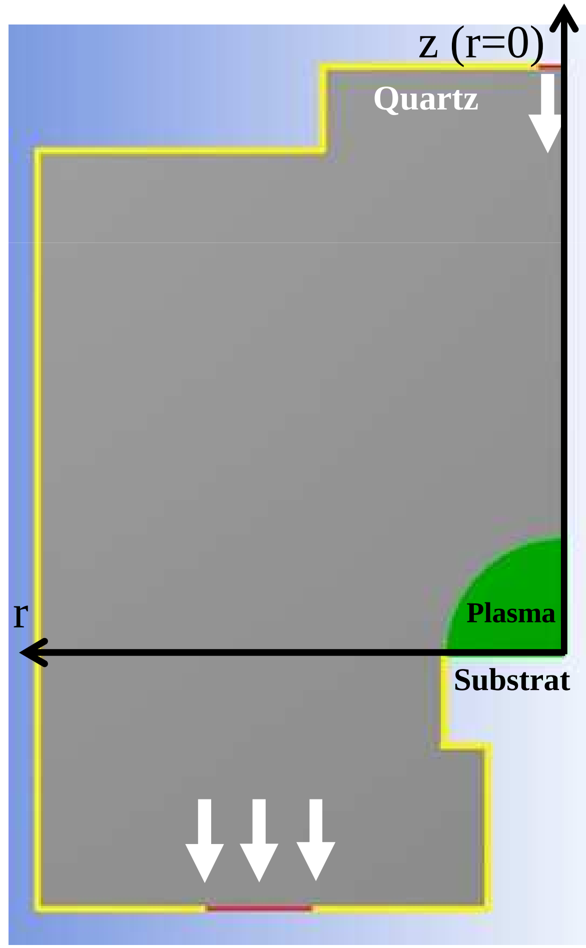

# Principe du modèle 1-D

✓ Modèle thermo-chimique du plasma hors-équilibre :

- 2 modes d'énergie : $T_g$ et fdee
- Pour les plasmas $H_2$ : 8 espèces / 29 réactions
- Pour les plasmas $H_2/CH_4$ : 28 espèces / 131 réactions

$H_2$, H(n=1-3), $H_{1\text{-}3}^+$, $CH_{0\text{-}4}$, $C_2H_{0\text{-}6}$, $CH_{3\text{-}5}^+$, $C_2H_{2\text{-}6}^+$, $e^-$

✓ Paramètres d'entrée : Densité de puissance, composition du gaz, épaisseurs de couches limites pour $T_g$, H, et les autres espèces

✓ Transport = Diffusion

3 types d'équations :

✓ Continuité : $\boxed{\frac{dY_s}{dt} = \frac{W_s}{\rho} - \frac{1}{\rho}.\left(\frac{1}{r}.\frac{d(r.F_r)}{dr}\right)}$ => [X]

✓ Energie des électrons : $\boxed{\frac{\partial \tilde{E}_e}{\partial t} = [PMW - Q_{e-v} - Q_{e-t} - Q_{e-X}]\frac{1}{\rho} - \left[\frac{1}{r}.\frac{d}{dr}\left(r.F_r^{(NRJe)}\right)\right].\frac{1}{\rho}}$ => $T_e$

✓ Energie totale : $\boxed{\frac{\partial \tilde{E}}{\partial t} = [PMW - Q_{rad} - S_P]\frac{1}{\rho} - \left[\frac{1}{r}.\frac{d}{dr}\left(r.F_r^{(NRJ)}\right)\right].\frac{1}{\rho}}$ => $T_g$

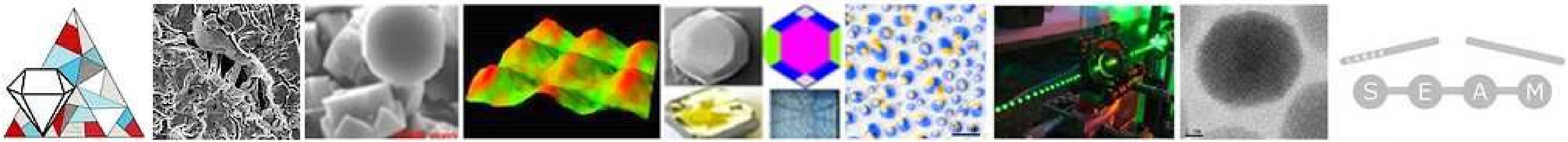




## Principe du modèle 2-D

Te, Tg, ne

**Module plasma**

8 espèces, 36 réactions

Tg, <ee>, ne,...

Iterations

**Module électromagnétique**

Equations de Maxwell

Mouvement électronique

E, H, Je-HF, MWPD

Densité de puissance micro-onde

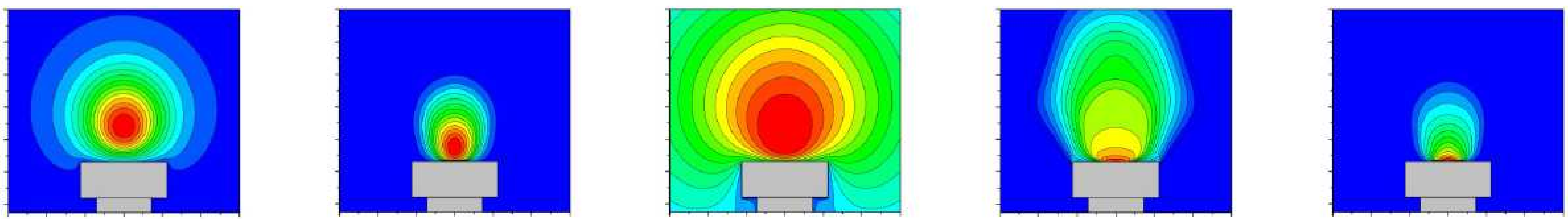

[H] ($cm^{-3}$) | Ne ($cm^{-3}$) | Tg (K) | Te (K) | MWPD ($W.cm^{-3}$)

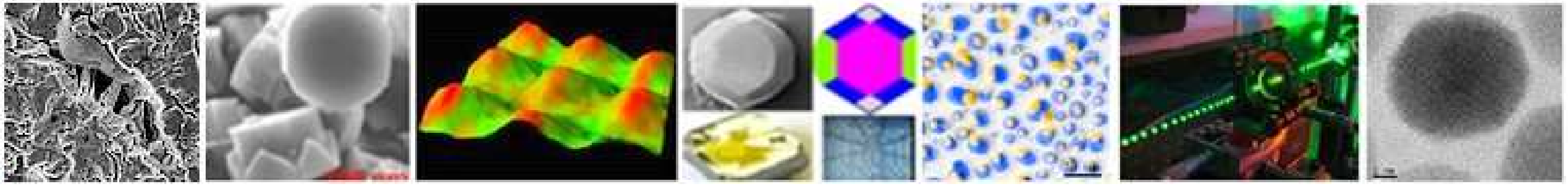



# $H_2/CH_4$ PLASMAS FOR POLY- AND MONO-CRYSTALLINE DIAMOND

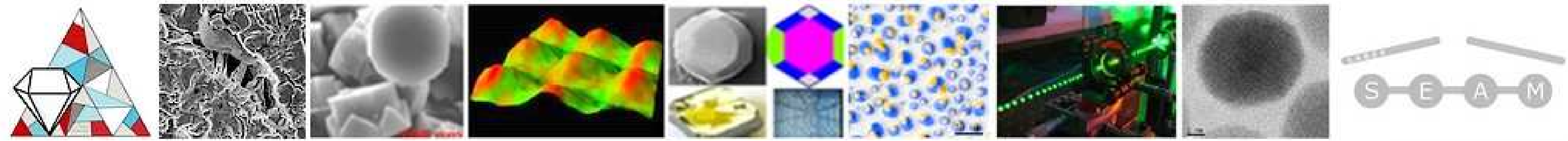




# $H_2/CH_4$ plasmas for poly- and mono- crystalline diamond

- **Example of studies (*)**: **Quantification of the methyl radical ($CH_3$)** by means of UV-Broadband Absorption spectroscopy and IR Tunable Diode Laser Absorption Spectroscopy

**Beer-Lambert absorption law:**

$$I(\nu) = I_0(\nu)\ exp\,(-\sigma_\lambda(T)\ l\ [CH_3])$$

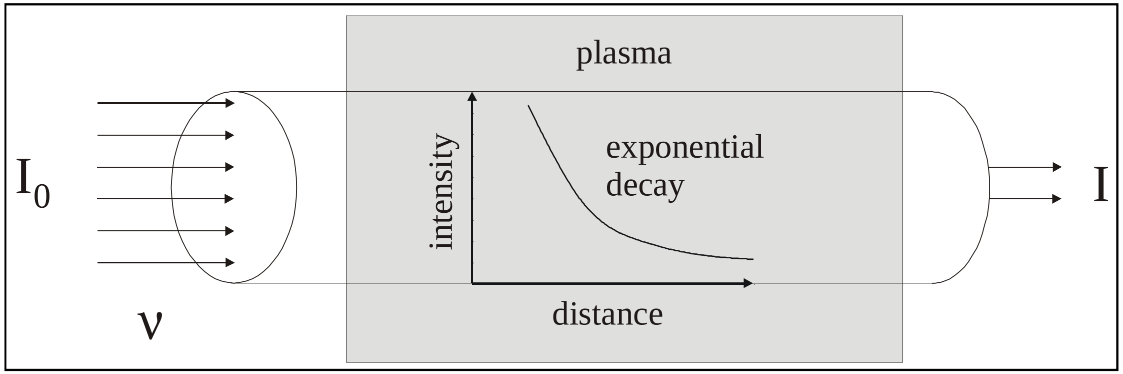


*$B(^2A_1') \leftarrow X(^2A_2'')$ electronic transition of $CH_3$ (216 nm)*

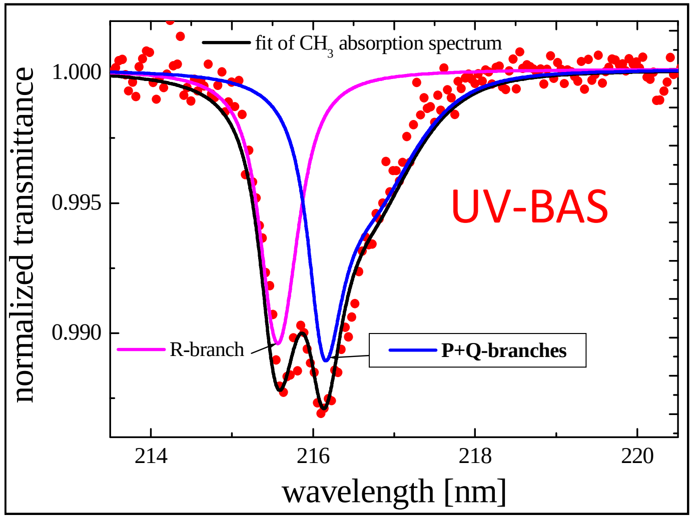


*Q(12,12) line of the $\nu_2$ band of $CH_3$ (612.41344 $cm^{-1}$)*

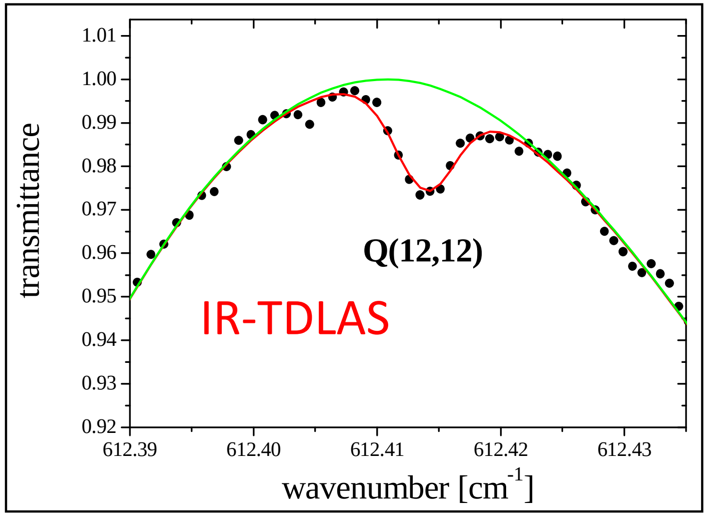




(*) G. Lombardi, G. D. Stancu, F. Hempel, A. Gicquel, J. Röpcke, PSST 2004 / PHC Procope 2001-2002

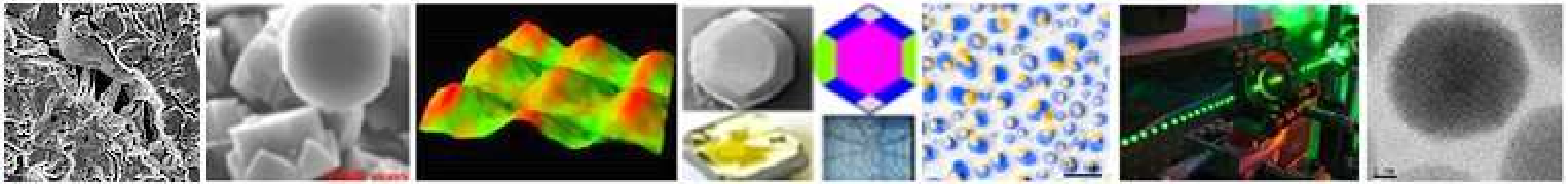

# LABEX SEAM

# $H_2/CH_4$ plasmas for poly- and mono- crystalline diamond

• **Analysis of the hydrocarbon chemistry** occurring in diamond deposition plasmas, by cross-comparison between IR TDLAS spectroscopic measurements and 1D-modeling (*)

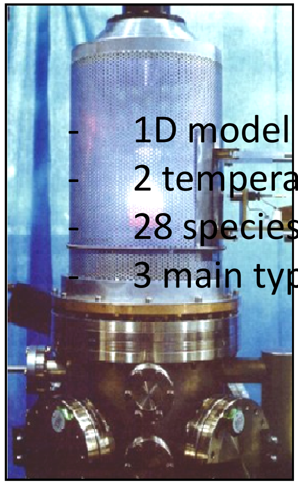

**Bell-jar reactor (2000's)**

Limited experimental conditions

- 1D model (axial or radial)
- 2 temperatures model: $T_g$, $T_e$
- 28 species and 131 reactions
- 3 main type of PDE (continuities, energy, electron energy)

**Metallic reactor (2010's)**

Extended experimental conditions

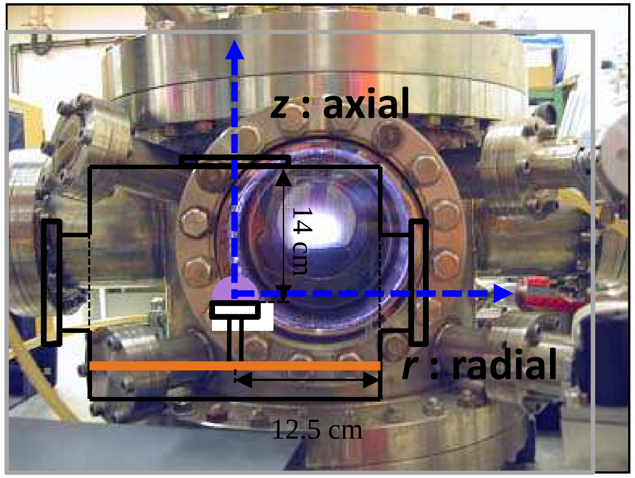


***$CH_4$ and $CH_3$ mole fractions***

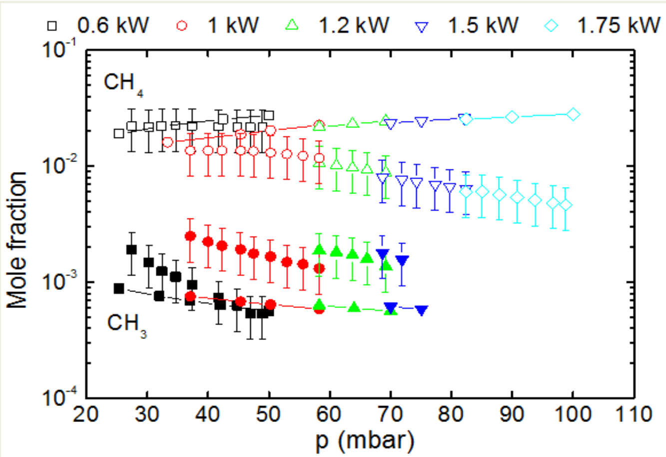


***Carbon containing species mole fractions*** *integrated along the* ***IR*** *optical path depending on the power ($H_2/CH_4$ (95:5))*

***Calculated values*** *from 1D average radial model shown by linked filled symbols*

***$C_2H_2$, $C_2H_4$ and $C_2H_6$ mole fractions***

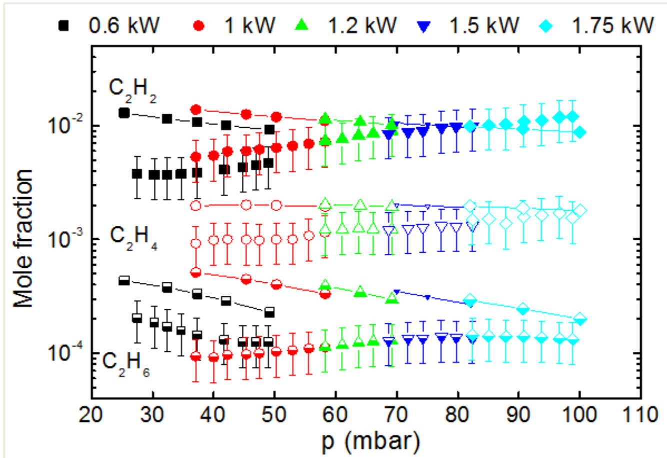


(*) G. Lombardi, K. Hassouni, G. D. Stancu, L. Mechold, J. Röpcke, A. Gicquel, PSST and JAP 2005
C. Rond, S. Hamann, M. Wartel, G. Lombardi, A. Gicquel, J. Röpcke, JAP 2015 / PHC Procope 2012-2013

# Composition du plasma selon l’axe de symétrie du réacteur

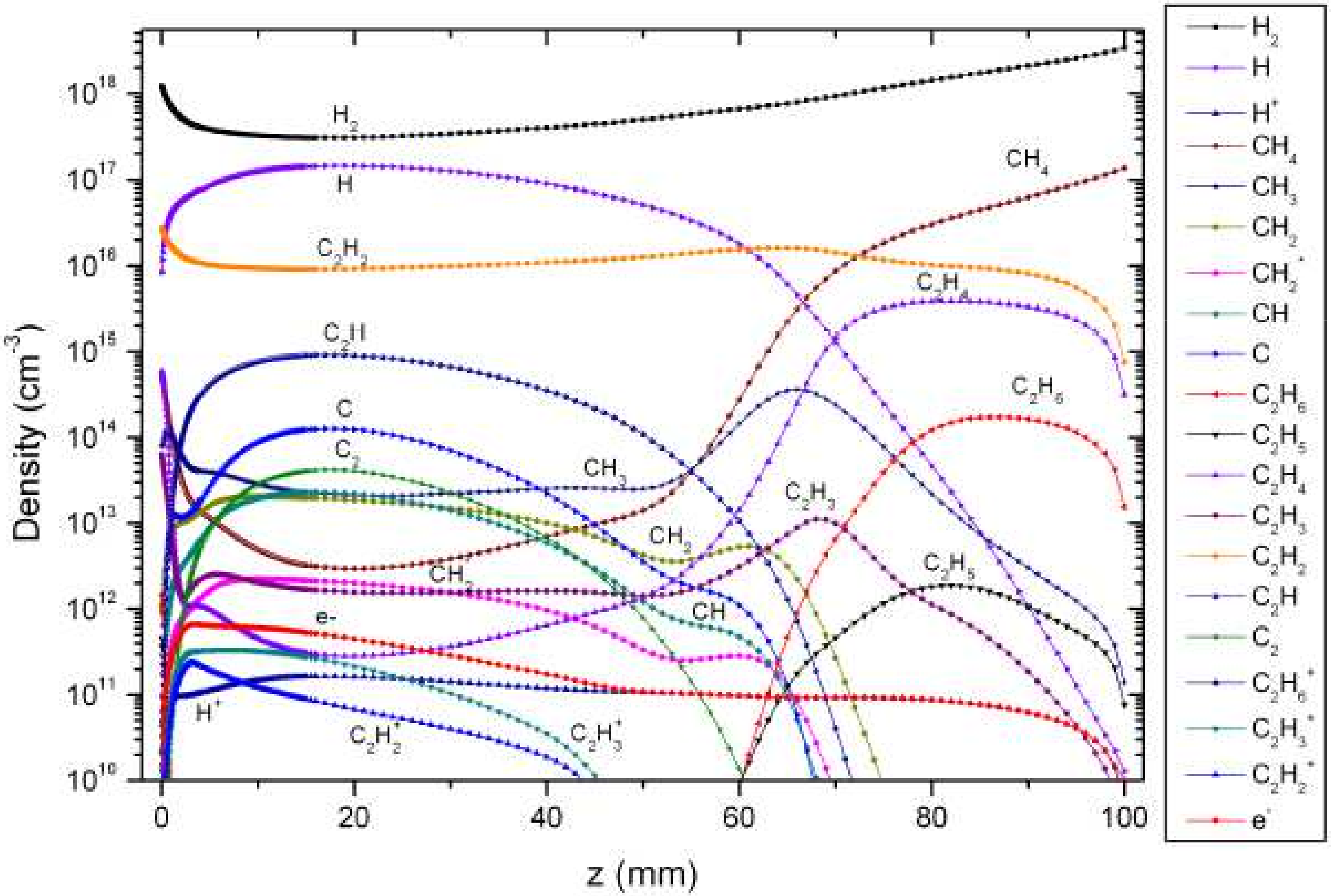

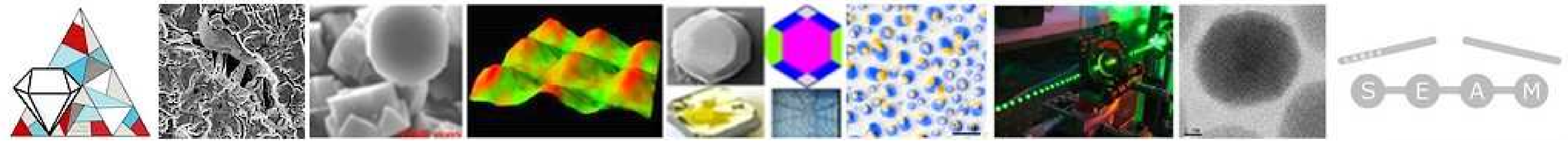



# Basse P => H et $CH_3$ produits dans le plasma

50 mbar
4% $CH_4$

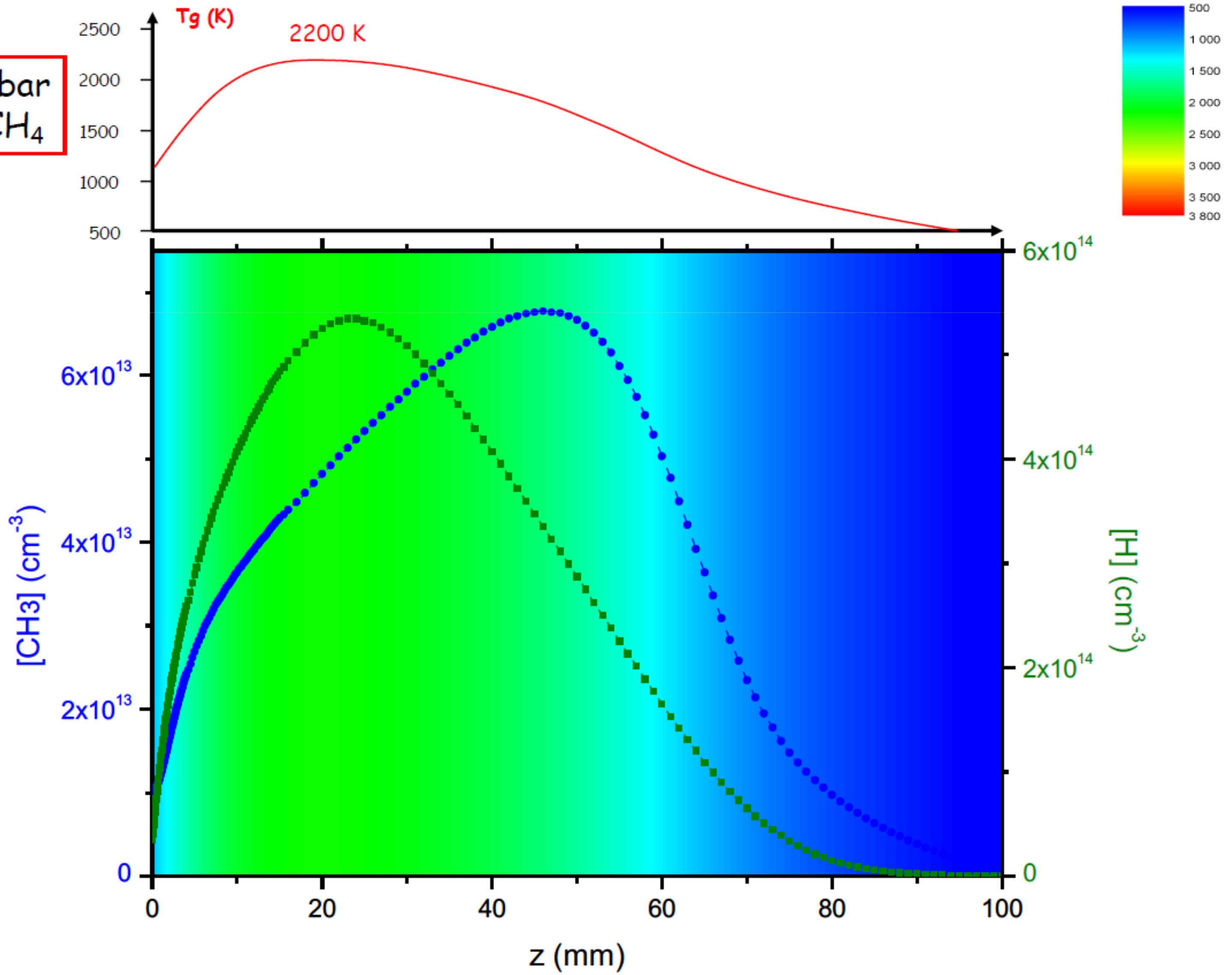

A haute pression, la production de H suit la température alors que $CH_3$ est confiné dans les zones plus froides

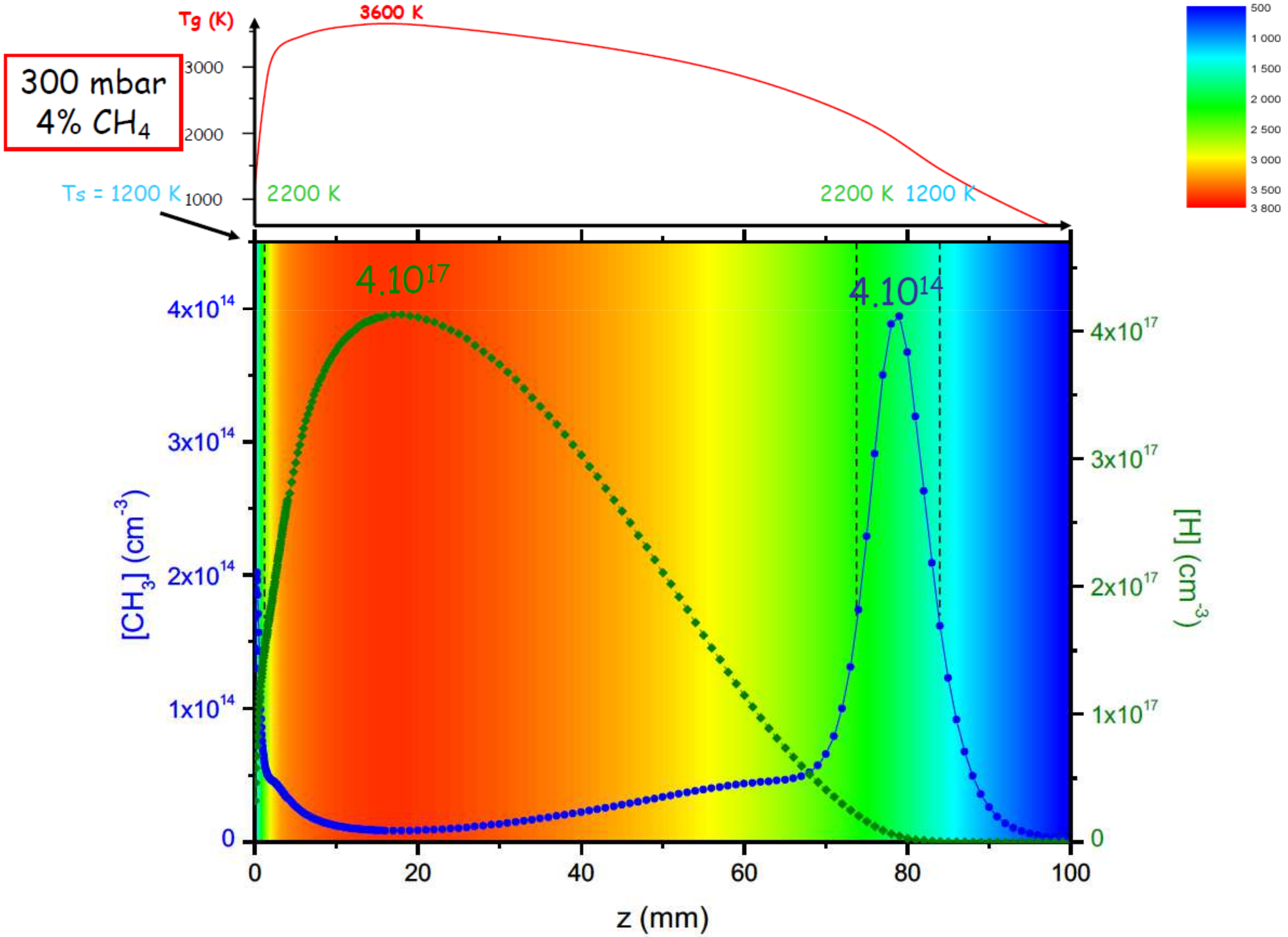

$CH_3$ est formé à une température de gaz dans la gamme 1200 – 2200 K

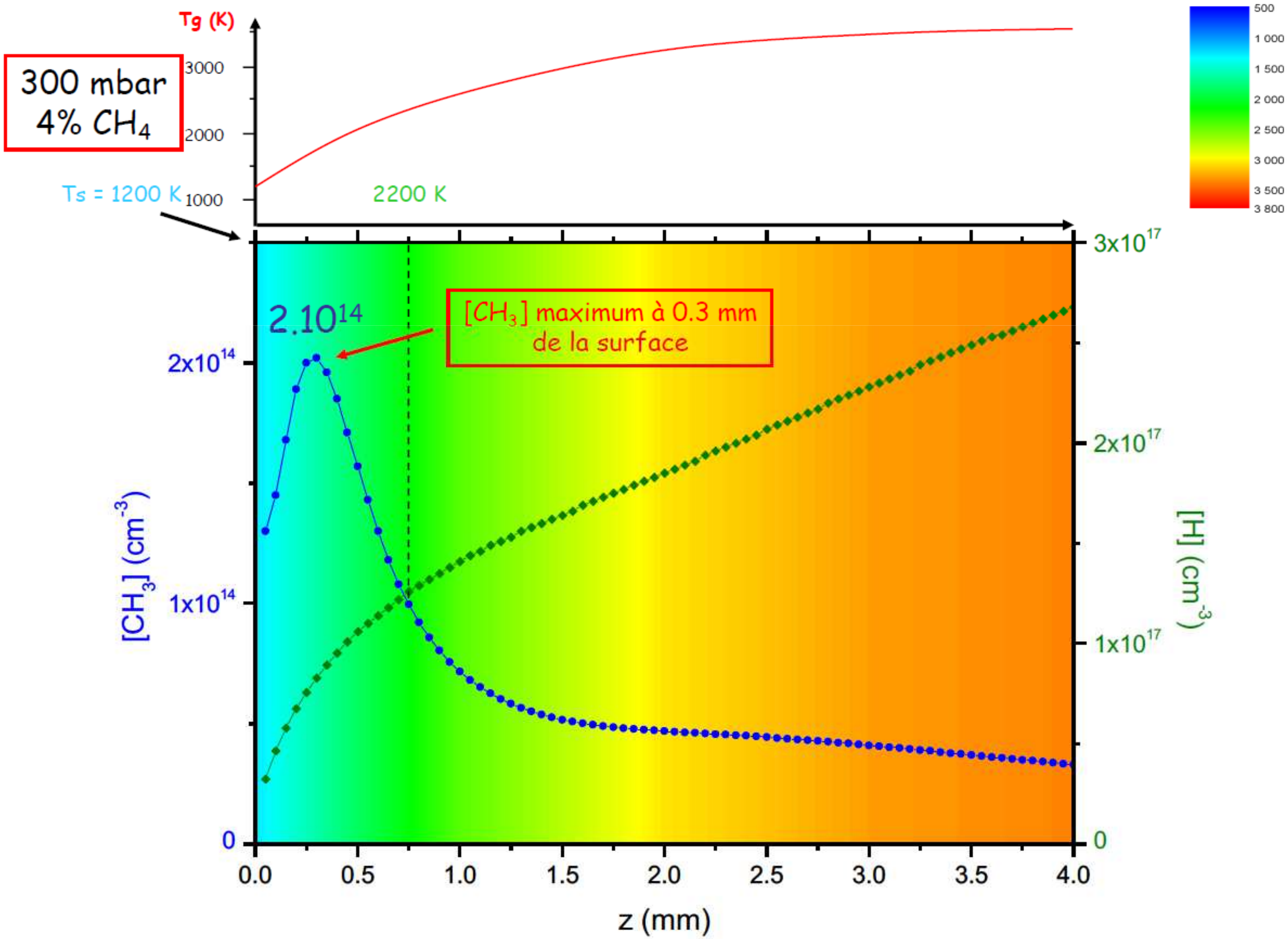

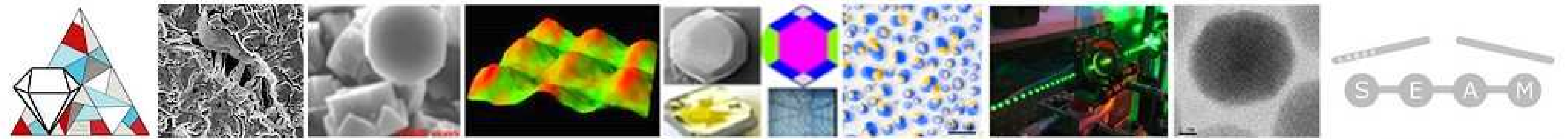




# ns two photon laser induced fluorescence (TALIF)

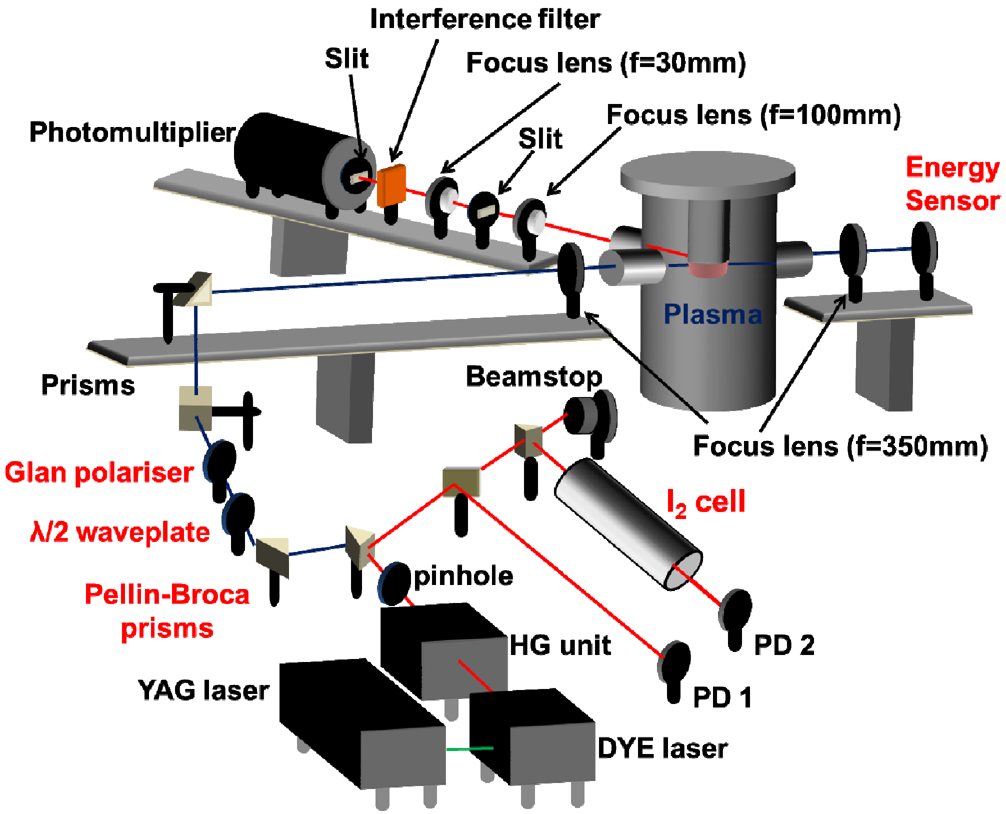


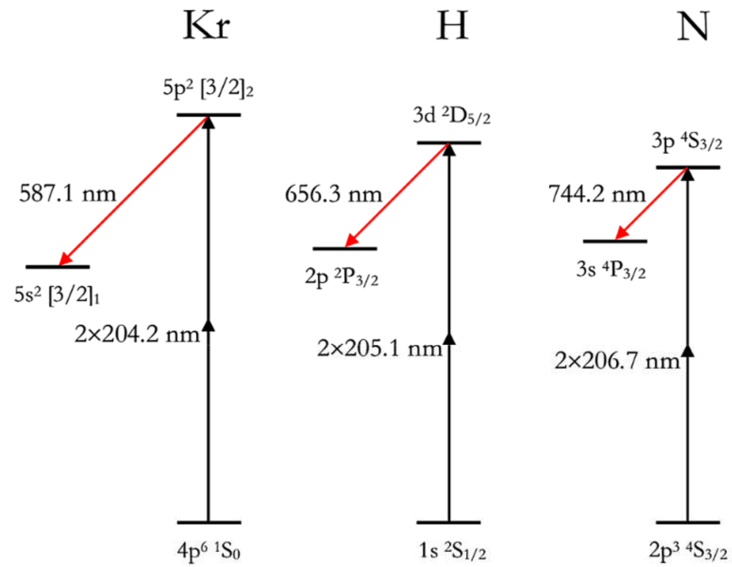


Transmission des filtres d'interférence à $\lambda_{Kr}$ et $\lambda_H$

Sections efficaces des collisions à deux photons.

$$n_H = \frac{\int_\nu \frac{S_{fluo\;H}(\nu)}{E^2_{laser_H}(\nu)}d\nu}{\int_\nu \frac{S_{fluo\;Kr}(\nu)}{E^2_{laser_{Kr}}(\nu)}d\nu}\frac{T_{Kr}}{T_H}\frac{\eta_{Kr}}{\eta_H}\frac{\sigma^{(2)}_{Kr}}{\sigma^{(2)}_H}\frac{\nu_H^2}{\nu_{Kr}^2}\frac{A_{Kr\;5p-5s}}{A_{H\;3-2}}\frac{\tau_{fluo\;Kr}}{\tau_{fluo\;H}}n_{Kr}$$

Sensibilité du système de détection à $\lambda_{Kr}$ et $\lambda_H$

Coefficient d'Einstein d'émission spontanée pour les transitions examinées

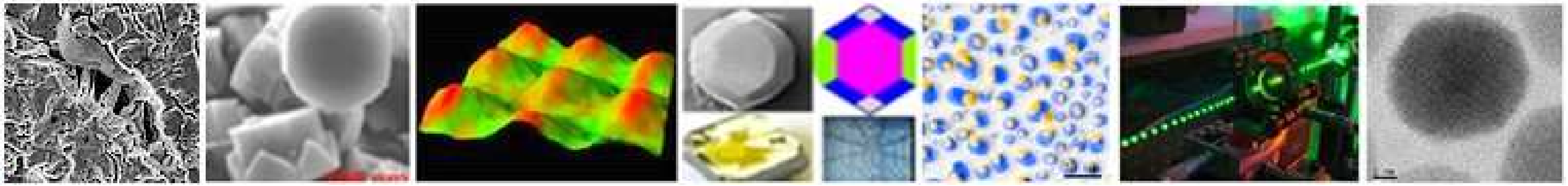



# H atoms temperature

- Gas temperature needed for :
  - quenching coefficients
  - $H_2$ density

- H atom temperature ~ gas temperature *

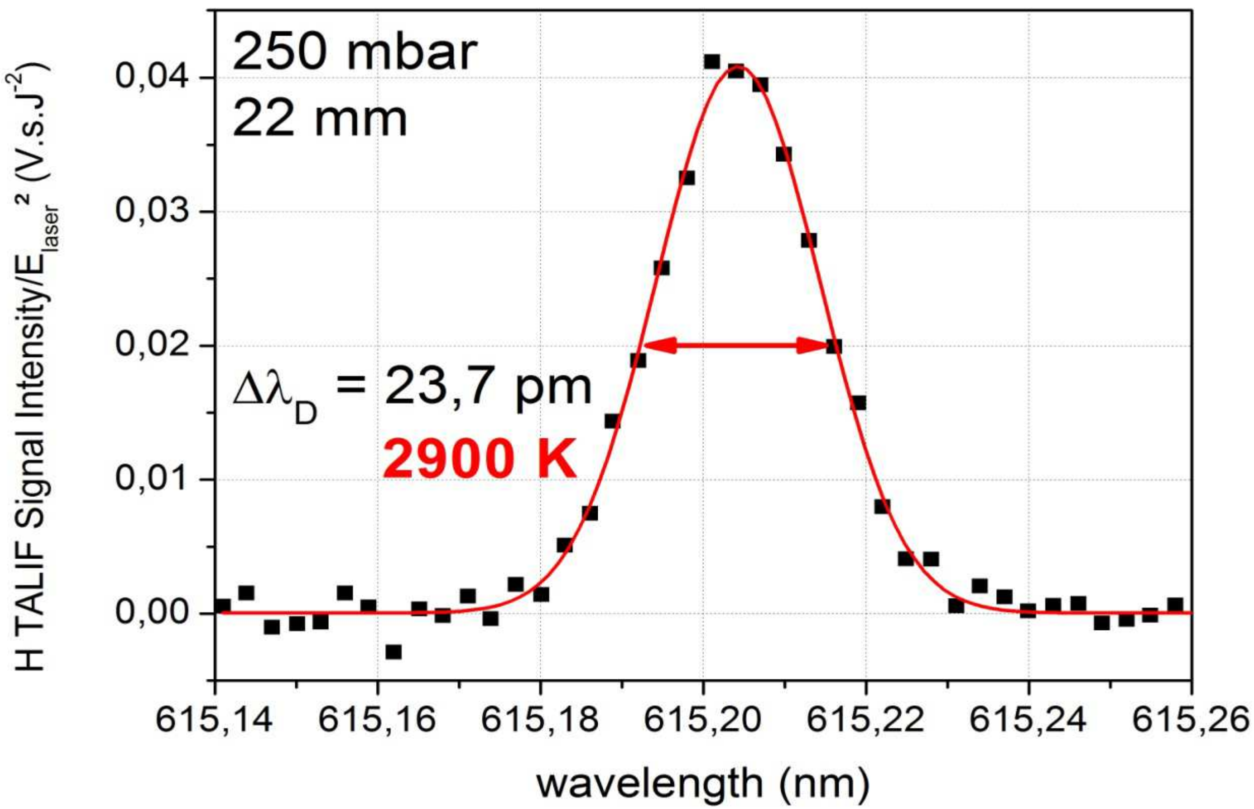


*A. Gicquel *et al., Diamond and related materials* ***5 (1996) 366-372***

# H atoms density

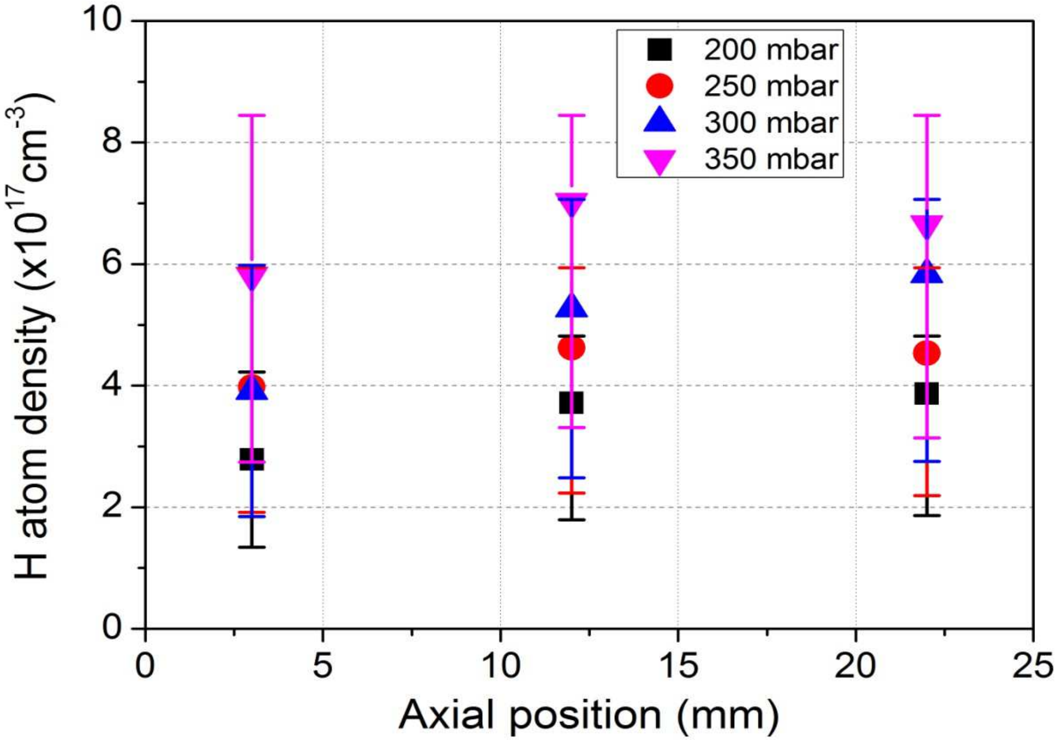


$H_2$ 99% - $CH_4$ 1% 3000 W

**Dissociation of $H_2$ :**

**> 55 % at 3 mm**

**> 75 % at 12 and 22 mm**

# 2D $H_2$-$CH_4$ Self-consistent model

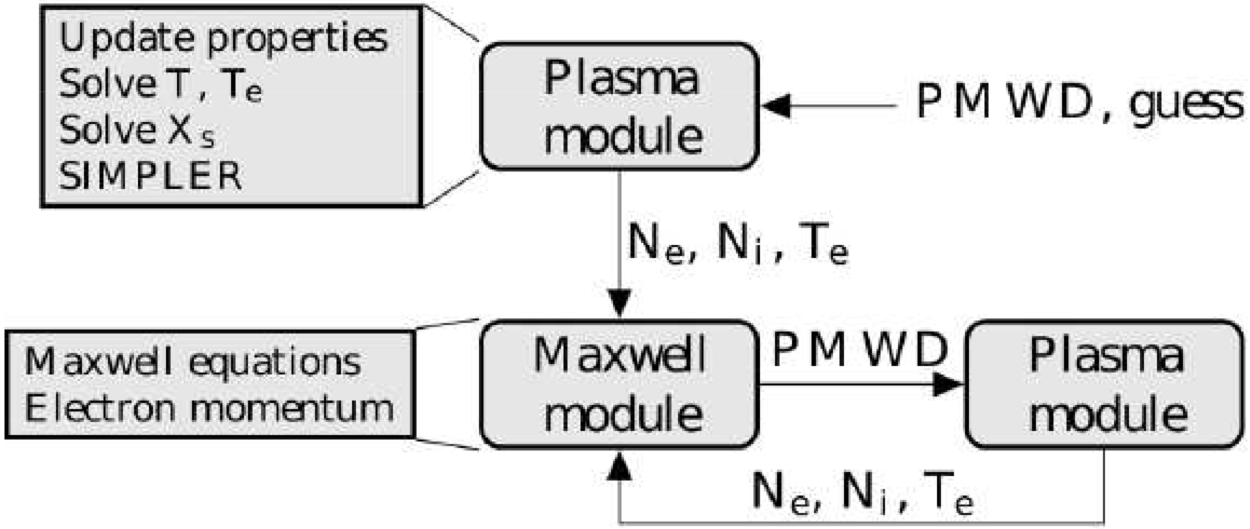


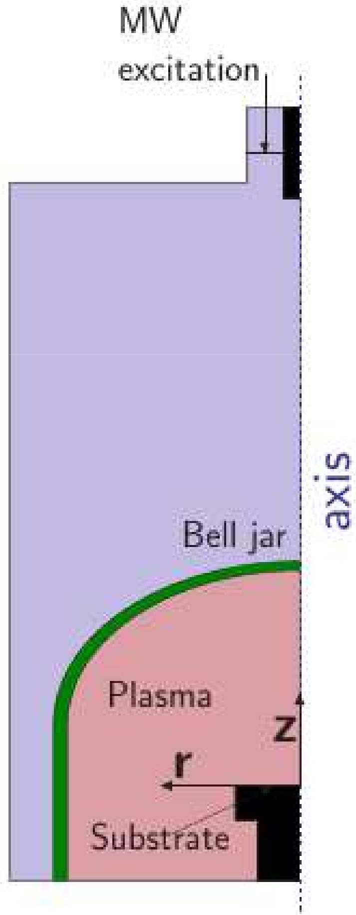

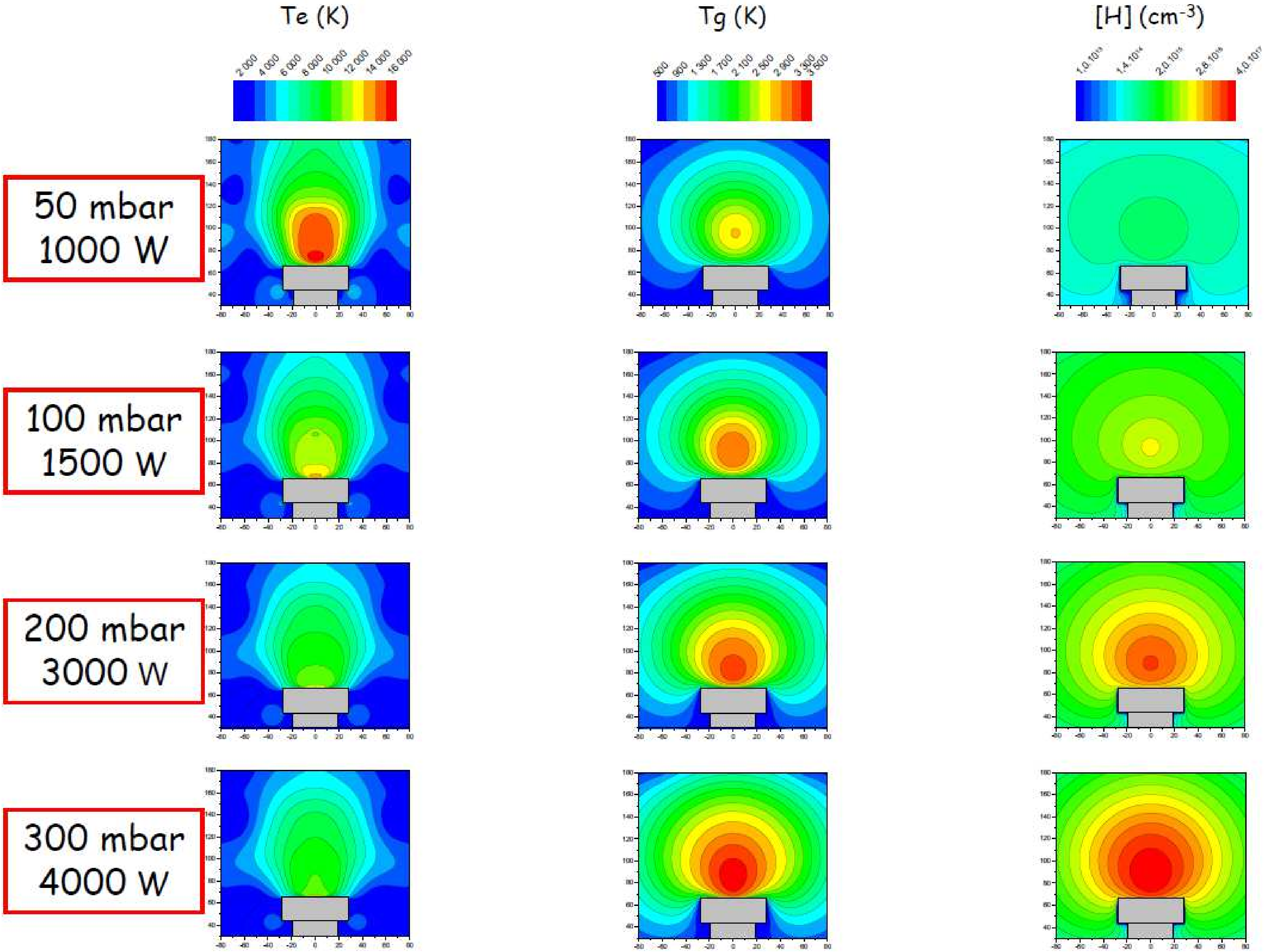


Te : 15 000 ⇨ 10 000 K     Tg : 2200 ⇨ 3600 K     [H] : $5.10^{14}$ ⇨ $4.10^{17}$ $cm^{-3}$

*F. Silva et al., J. Phys.: Condens. Matter* ***21*** *(2009) 364202*

# Hydrodynamic effects

Stability of plasma in MW reactor at 200 mbar

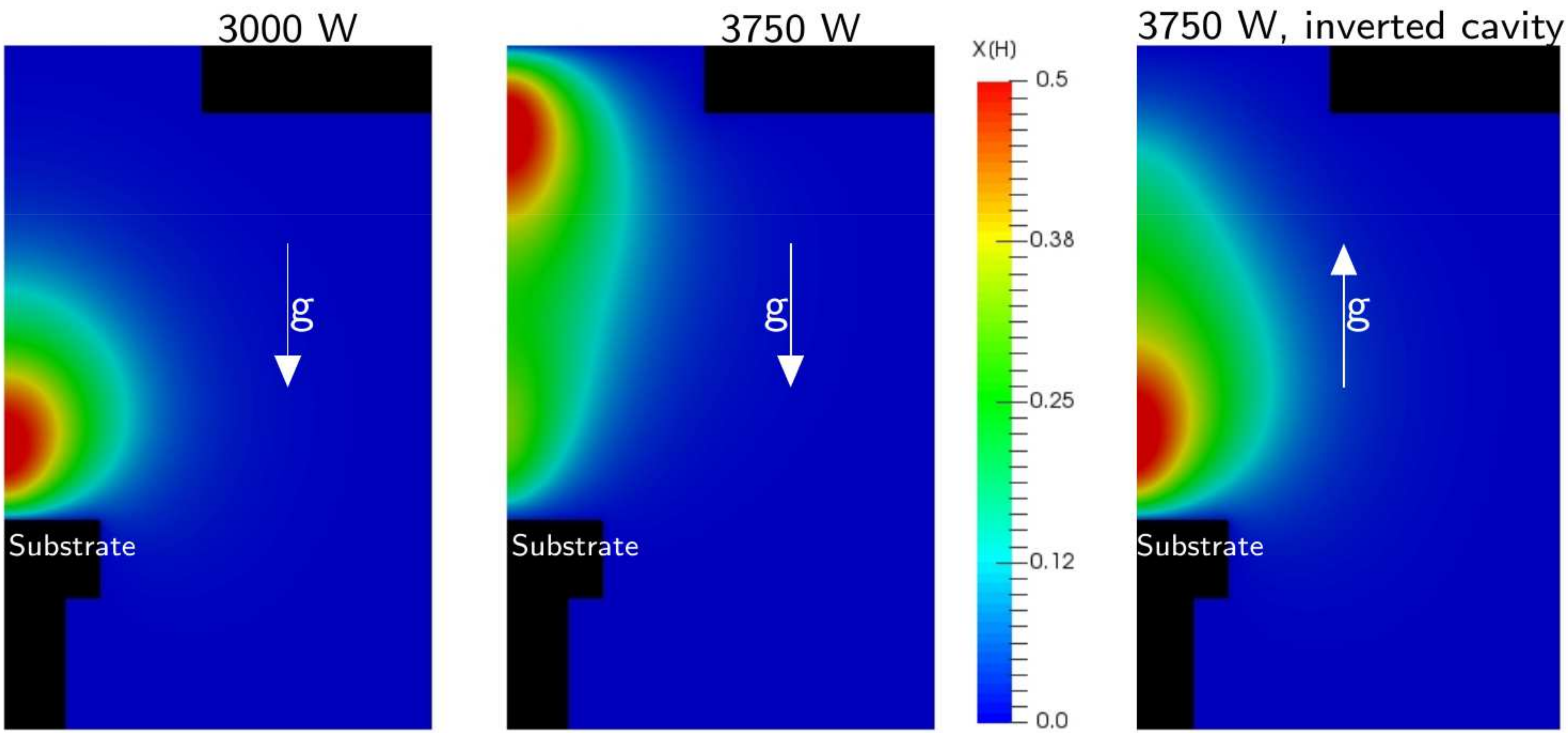

LABEX SEAM

# Hydrocarbon densities

28 species 104 Reactions

First self-consistent simulations for $CH_4+H_2$ plasmas

Conditions: 200 mbar and 2500 W and 4% $CH_4$

$CH_3$ concentration

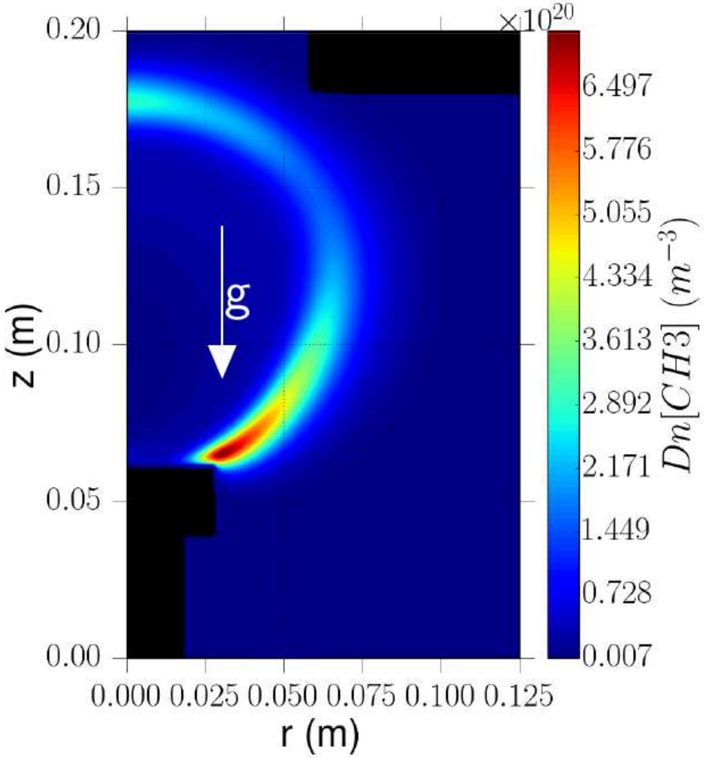


$C_2H_2$ concentration

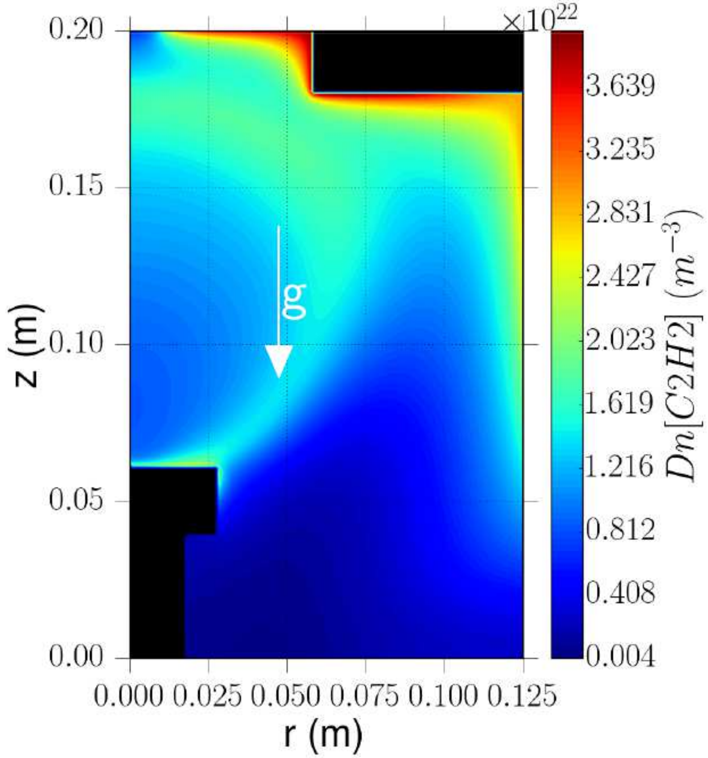

# Effect of methane on stability of MW reactor

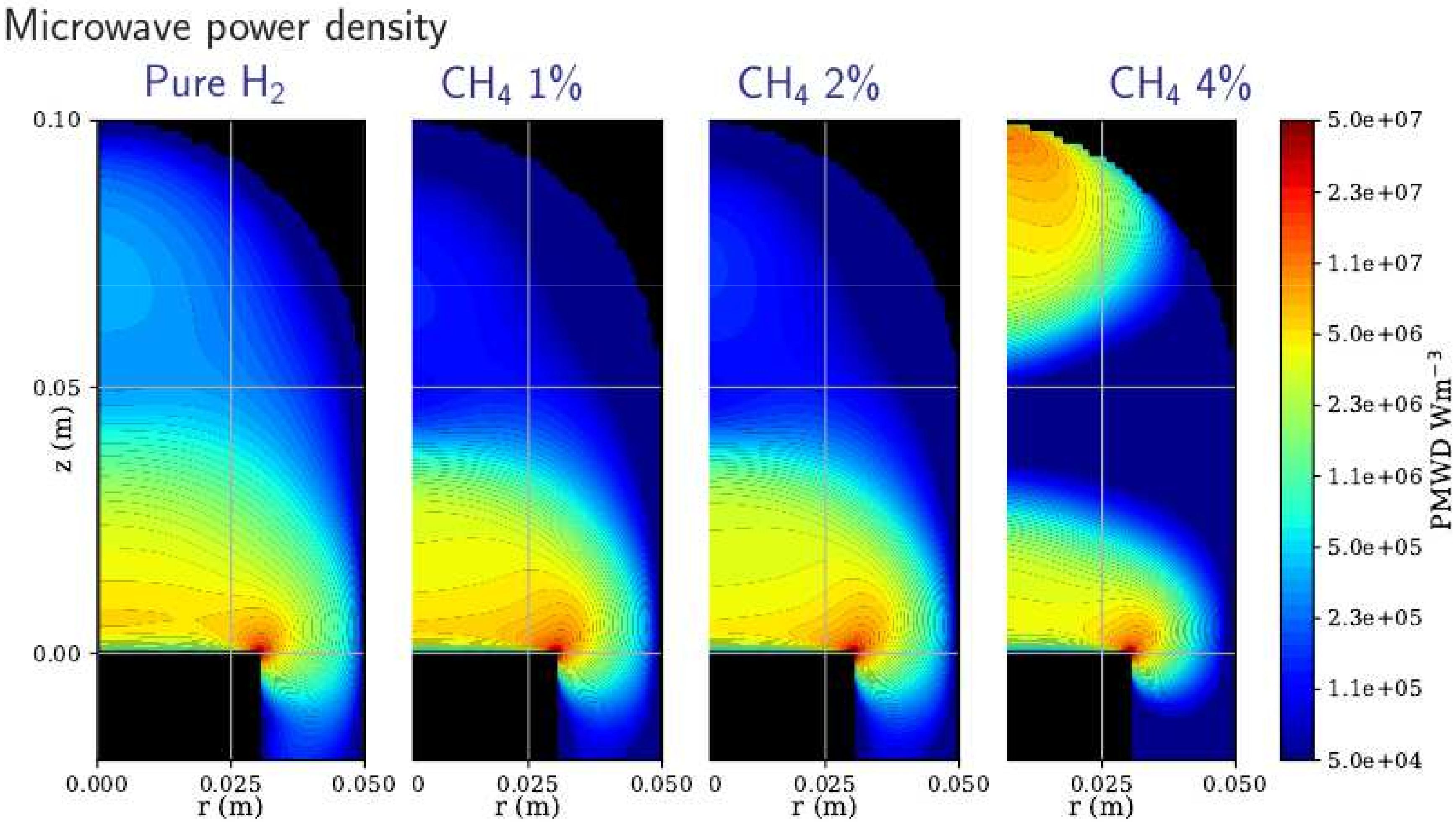

# Effect of methane on stability of MW reactor

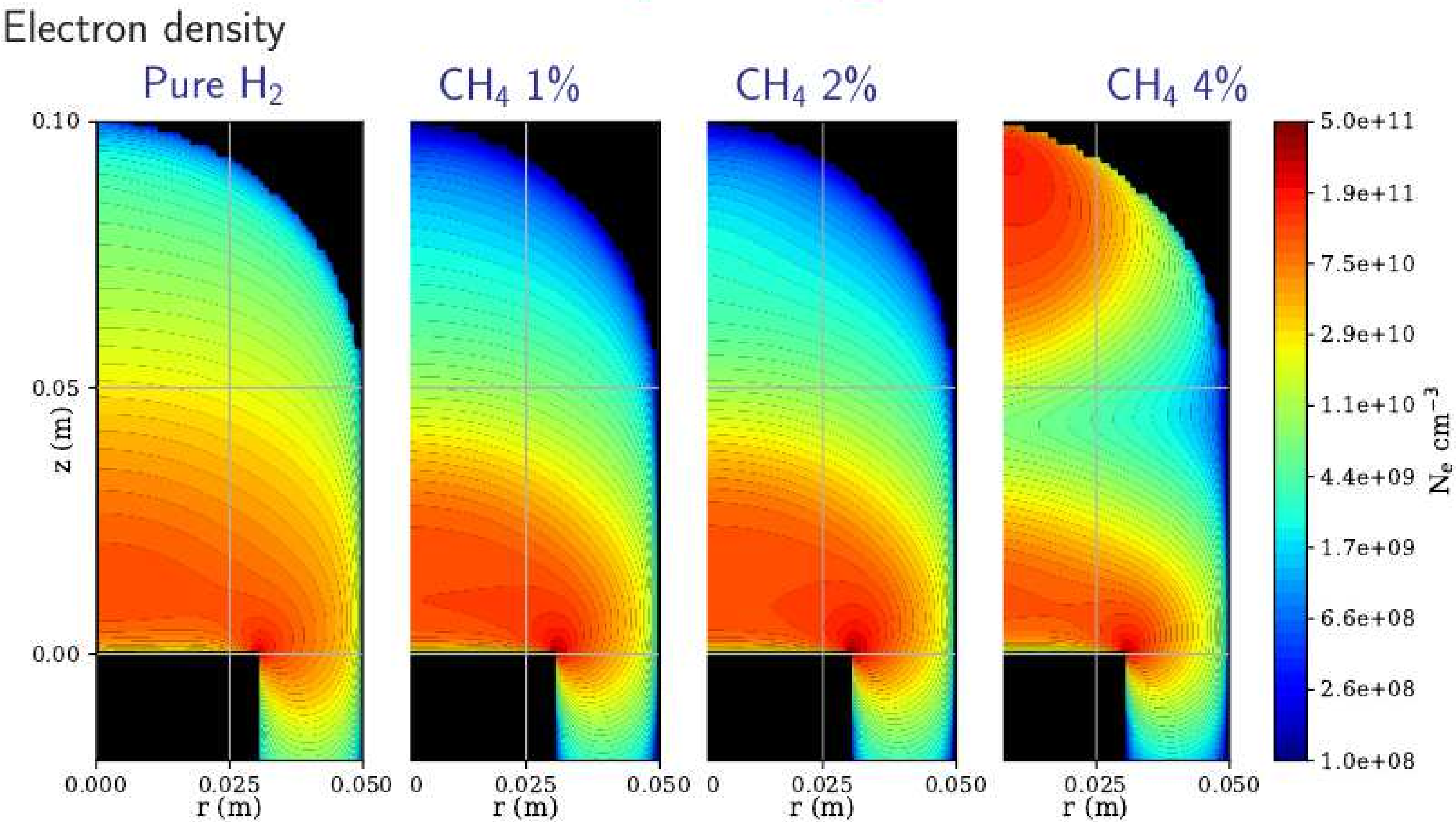

# Effect of methane on stability of MW reactor

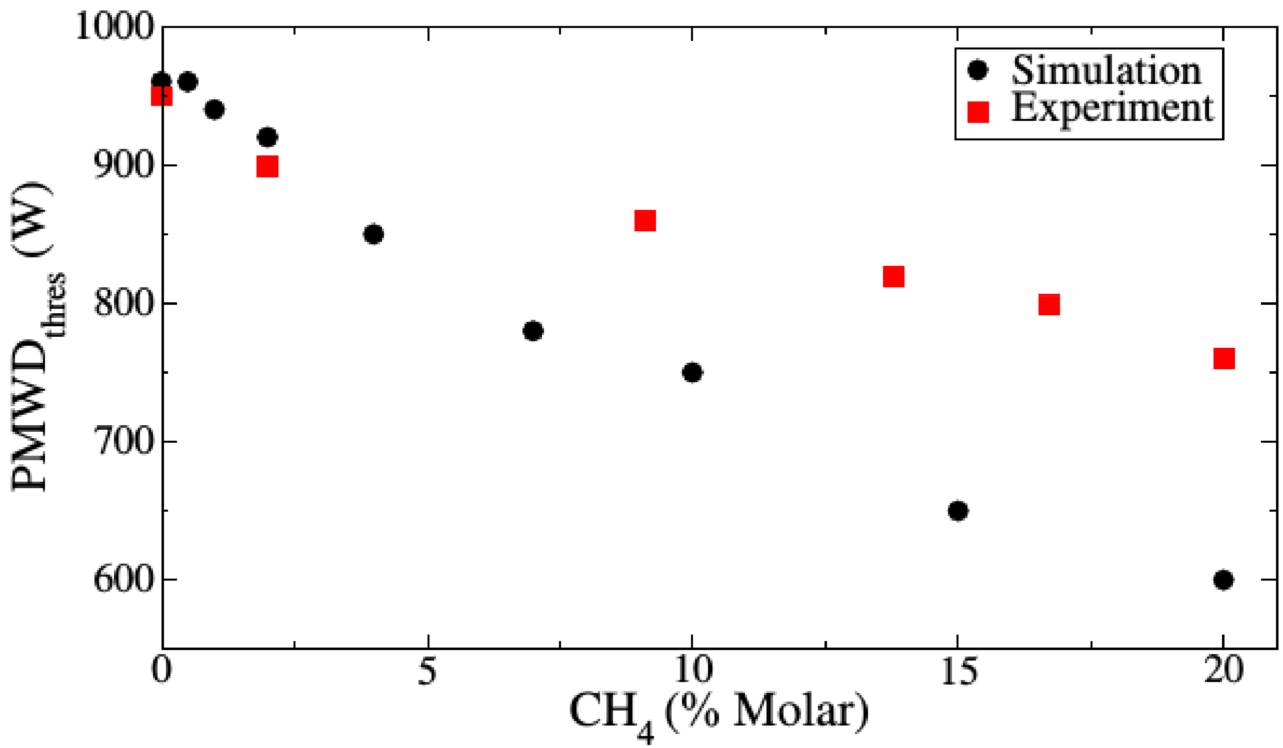


Threshold MW power at which transition from one ball to two ball plasma takes place as a function of methane concentration. Experiments and simulations

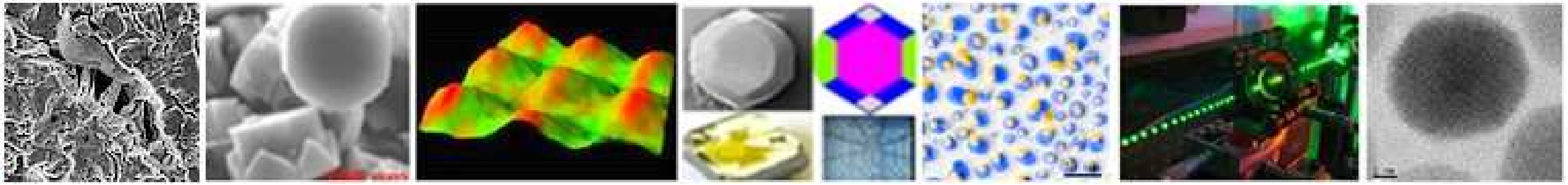

# $H_2/CH_4/B_2H_6$ DISCHARGES FOR P-DOPED DIAMOND

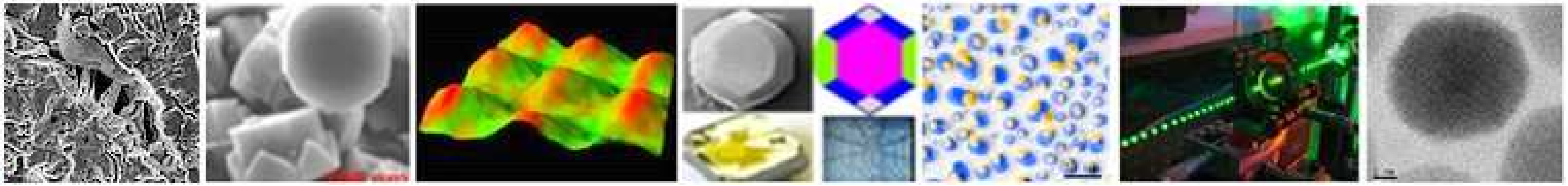

LABEX SEAM

# $H_2/CH_4/B_2H_6$ discharges for p-doped diamond

**Boron** = p-type dopant (holes)

**Objective => Grow thick layers with high B-doping for vertical Schottky diode**

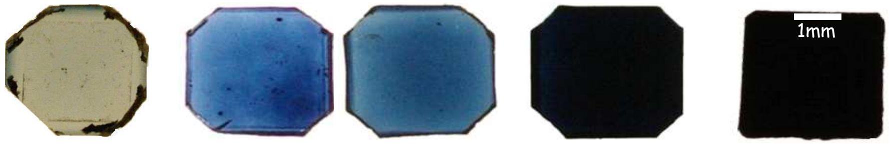


| $(B/C)_{gas}$ | 120 ppm | 800 ppm | 2000 ppm | 5000 ppm | 6000 ppm |
|---|---|---|---|---|---|
| Thickness : | 260 µm | 150 µm | 210 µm | 100 µm | 200 µm |

*Degree of decomposed $B_2H_6$ depending on pressure and power for different admixtures of $B_2H_6$ to the hydrogen feed gas (*)*

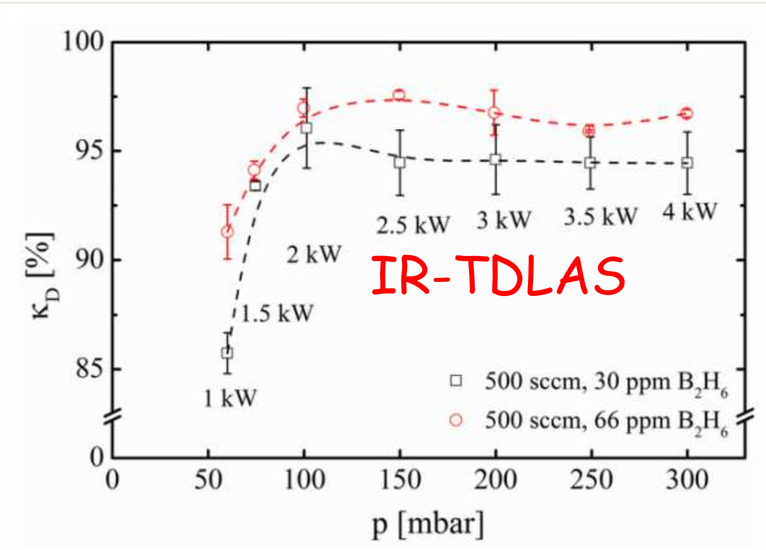


*Density of atomic boron depending on pressure and the power for different admixtures of $CH_4$ with a $B_2H_6$ content of 66 ppm (*)*

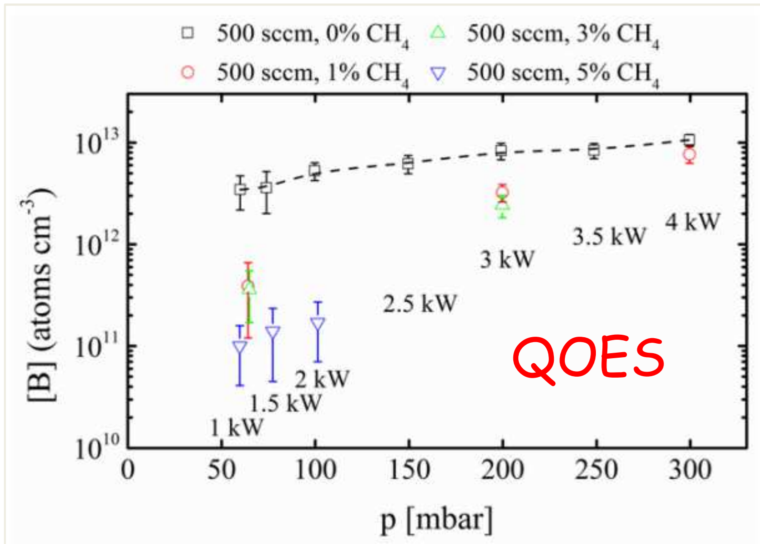


(*) S. Hamann, C. Rond, A.V. Pipa, M. Wartel, G. Lombardi, A. Gicquel, J. Röpcke PSST 2014 / PHC Procope 2012-2013
C. Rond, R. Salem, S. Hamann, G. Lombardi, J. Röpcke, A. Gicquel, PSST 2016 / PHC Procope 2012-2013

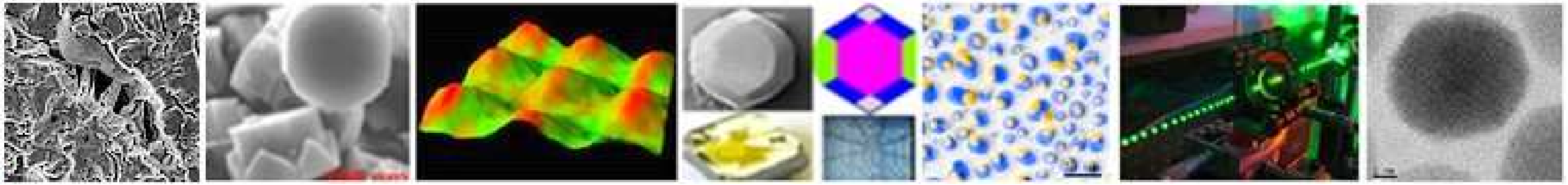



# Boron atom density (QOES)

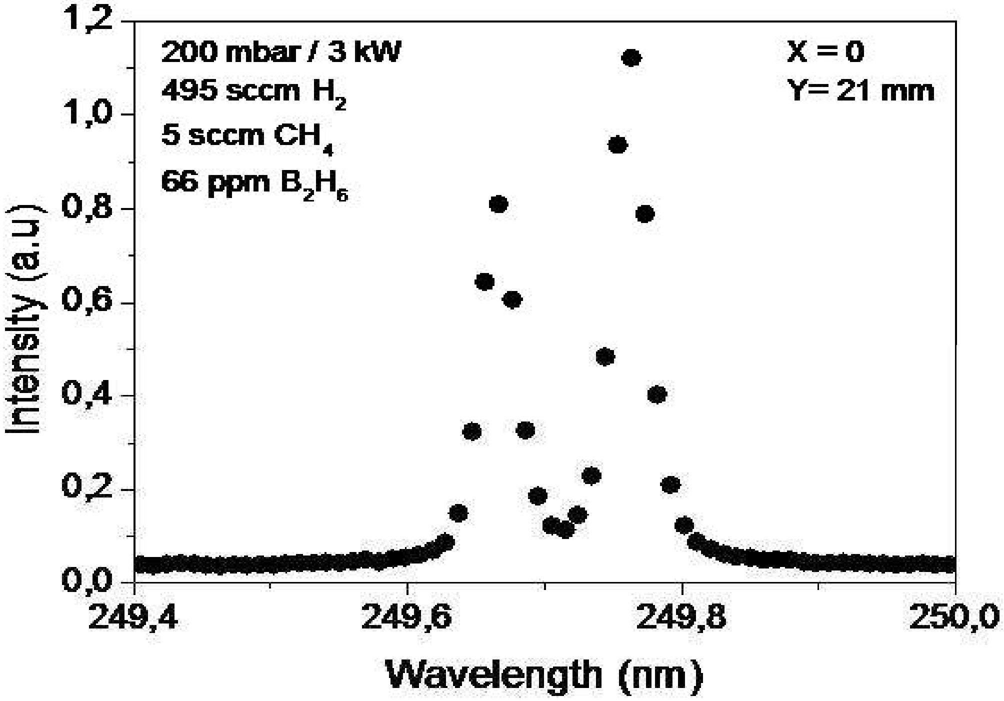


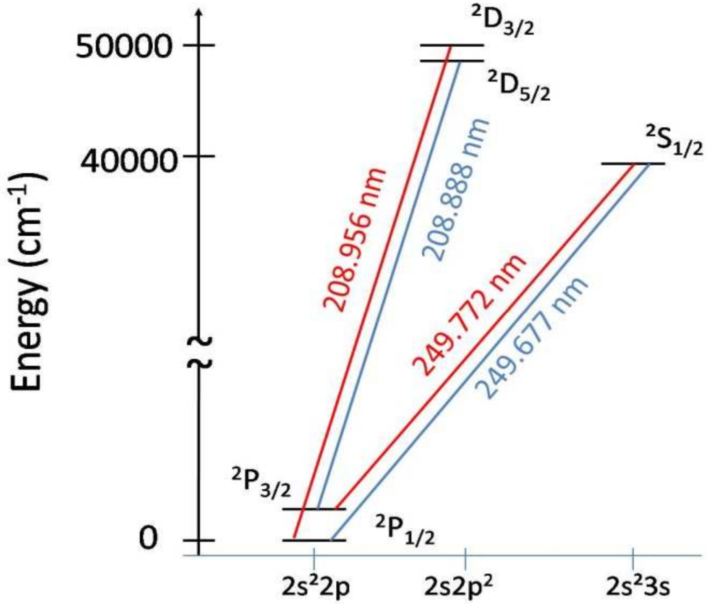


Optical Emission Spectroscopy :
$^2P_{3/2}$ level is two times more populated than the $^2P_{1/2}$ level
Oscillator strength are identical
249.772 nm line is more sensitive to self-absorption.

Boron density deduced from the ratio I(249.677)/I(249.772).

# Boron atom density (Absorption)

Hypothesis:
- Homogeneous plasma
- Similar emission and absorption profiles

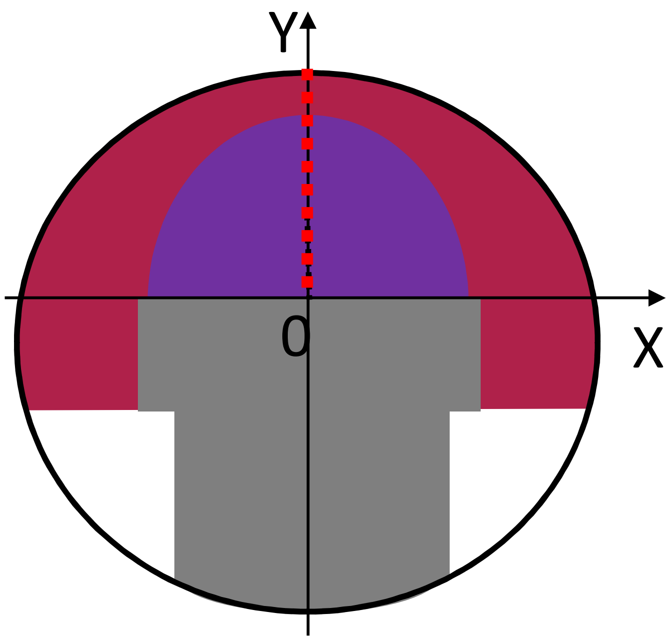


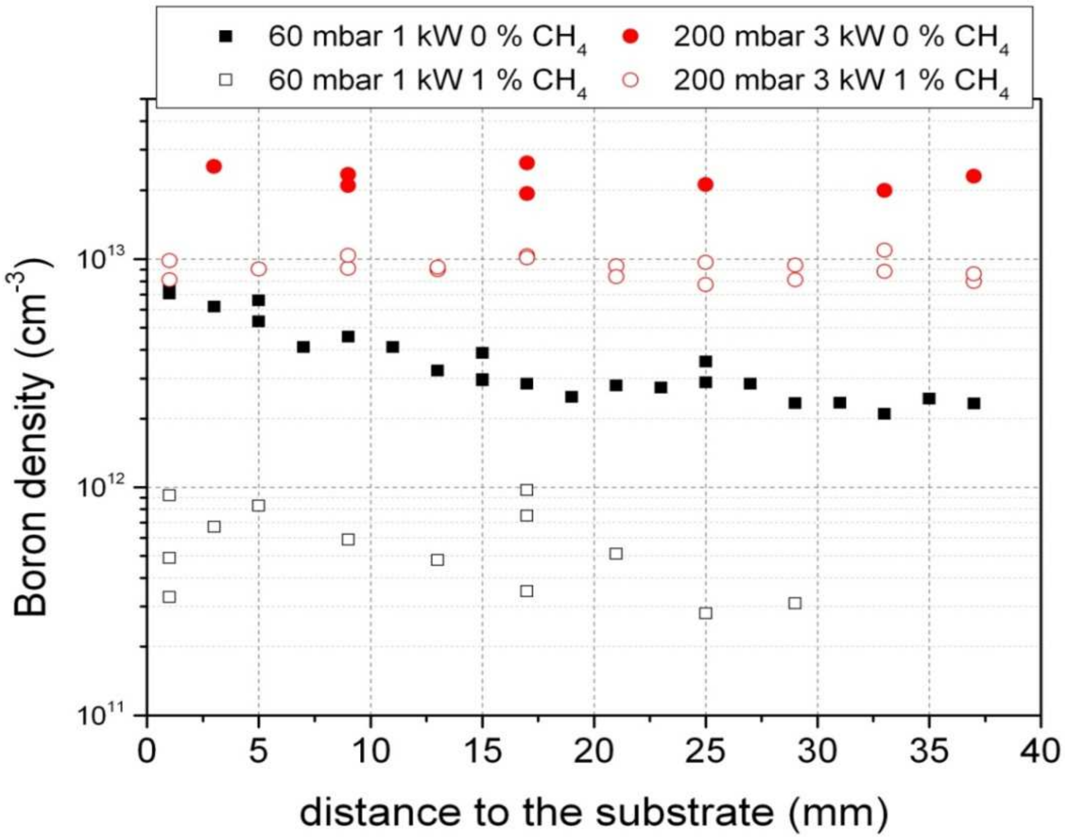


Measurements spatially integrated along the optical path

Absorption length = 5 cm

# LIF on Boron atoms

Advantages :
- Spatially resolved measurement compared to OES or OAS.
- Measurement of the ground state

Disavantages: almost no litterature about LIF  on B-atom

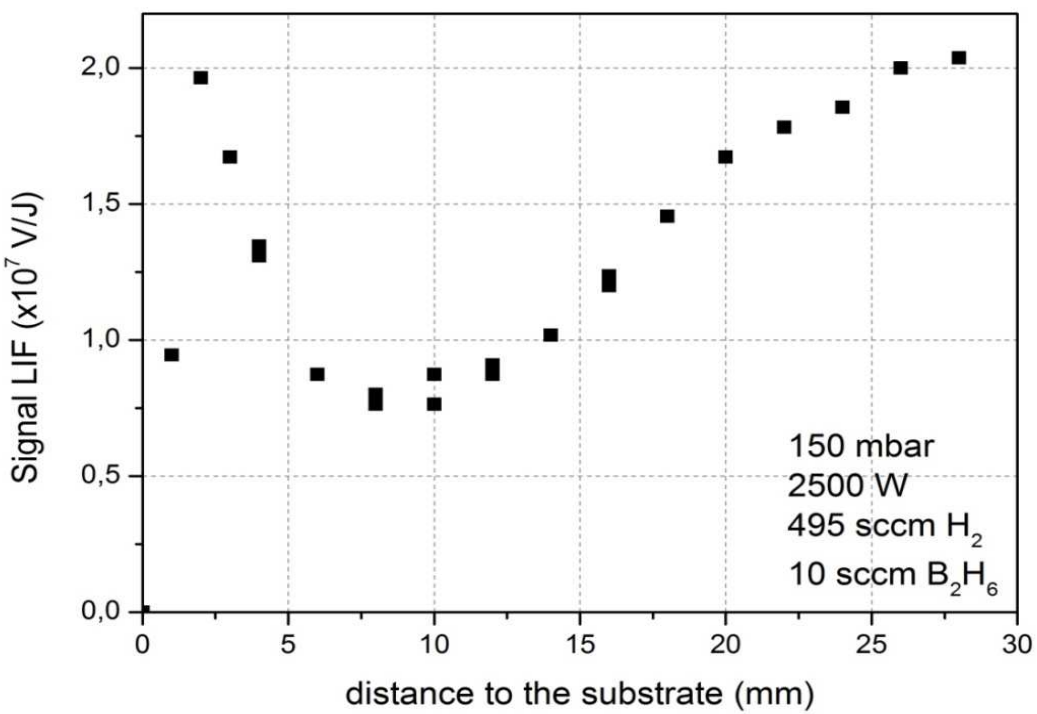


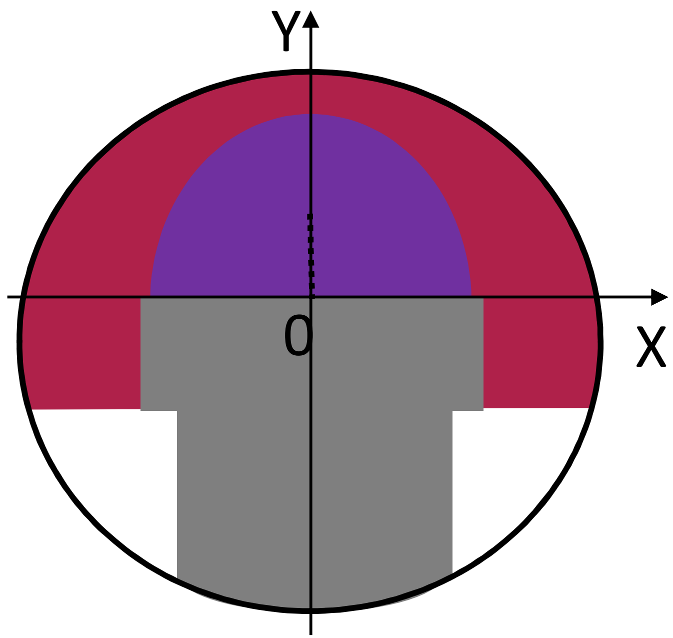


Minimum of fluorescence signal in the plasma ball
Unexpected results with respect to absorption measurements

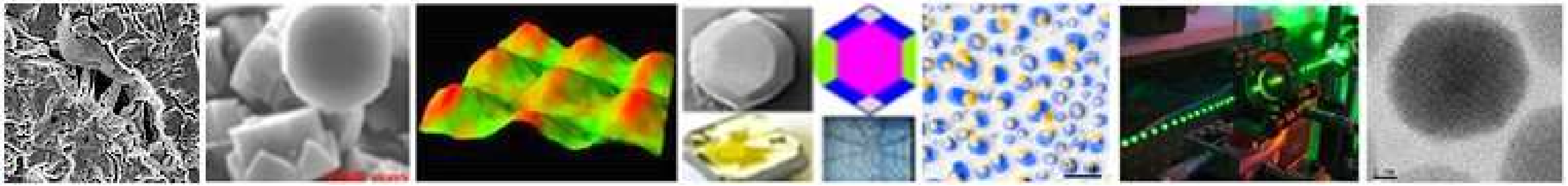



# $Ar/H_2/CH_4$ DISCHARGES FOR NANOCRYSTALLINE DIAMOND

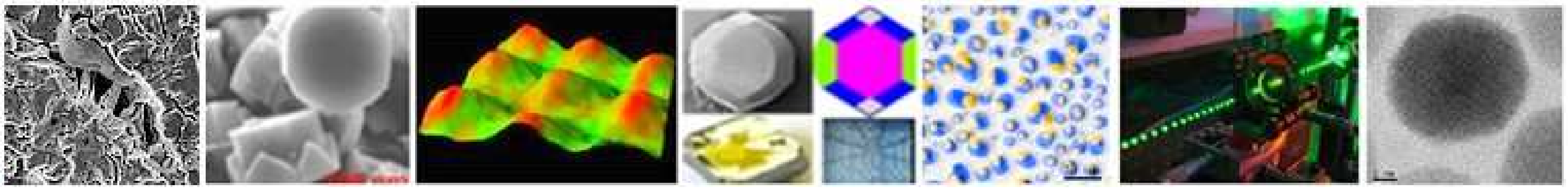

LABEX SEAM

# $Ar/H_2/CH_4$ discharges for nanocrystalline diamond

- **Interesting** **low roughness** **properties of Nano-Crystalline Diamond (NCD) => new applications**
- **Key parameters to control[(*)]:** Gas temperature and $C_2$ density (growth precursor)
- **Example** **of results in a Bell-jar reactor (2000's)**

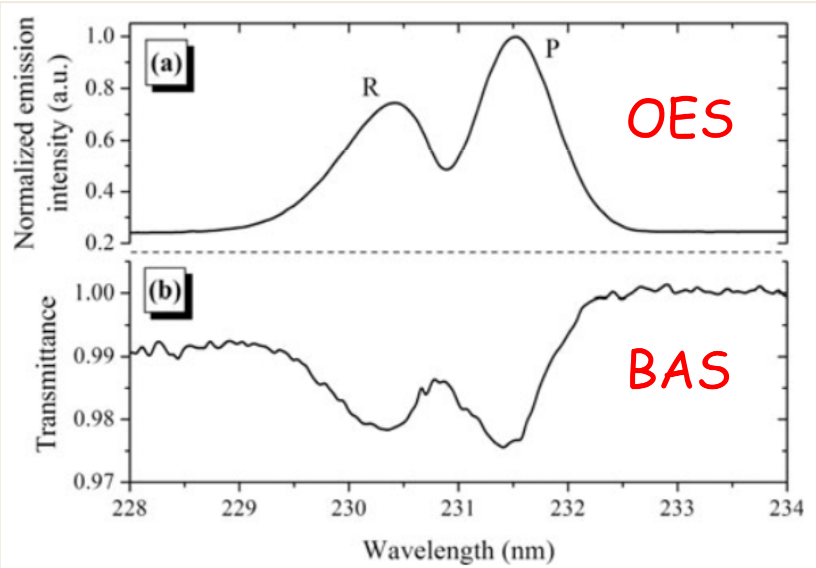


*Typical examples of spectra obtained around 231 nm for the* ***$C_2$ ($D^1\Sigma_u^+$-$X^1\Sigma_g^+$) Mulliken system*** *for a 97:2:1-500W (200 mbar) $Ar/H_2/CH_4$ plasma. (a) $D^1\Sigma_u^+ \rightarrow X^1\Sigma_g^+$ emission spectrum. (b) $D^1\Sigma_u^+ \leftarrow X_1\Sigma_g^+$ absorption spectrum.*

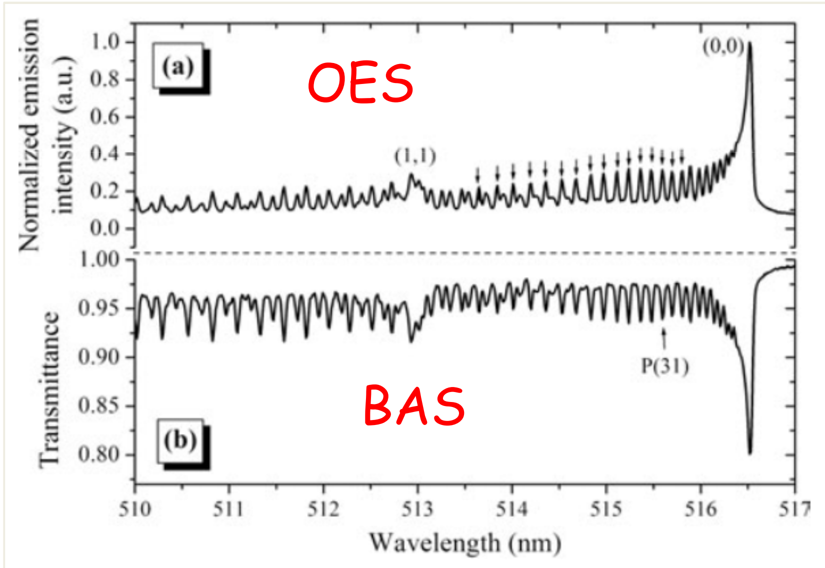


*Typical examples of spectra obtained at 516.5 nm for the* ***$C_2$ ($d^3\Pi_g$-$a^3\Pi_u$) Swan system*** *for a 97:2:1-500W (200 mbar) $Ar/H_2/CH_4$ plasma. (a) $d^3\Pi_g \rightarrow a^3\Pi_u$ emission spectrum. (b) $d^3\Pi_g \leftarrow a^3\Pi_u$ absorption spectrum.*

(*) G. Lombardi, F. Bénédic, F. Mohasseb, K. Hassouni, A. Gicquel, PSST 2004

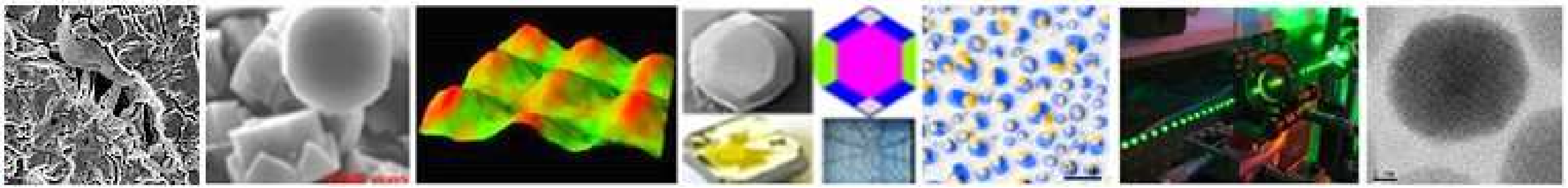



# $Ar/H_2/CH_4$ discharges for nanocrystalline diamond

- **Interesting low roughness properties of Nano-Crystalline Diamond (NCD) => new applications**
- **Key parameters to control(*):** Gas temperature and $C_2$ density (growth precursor)
- **Example of results in a Bell-jar reactor (2000's)**

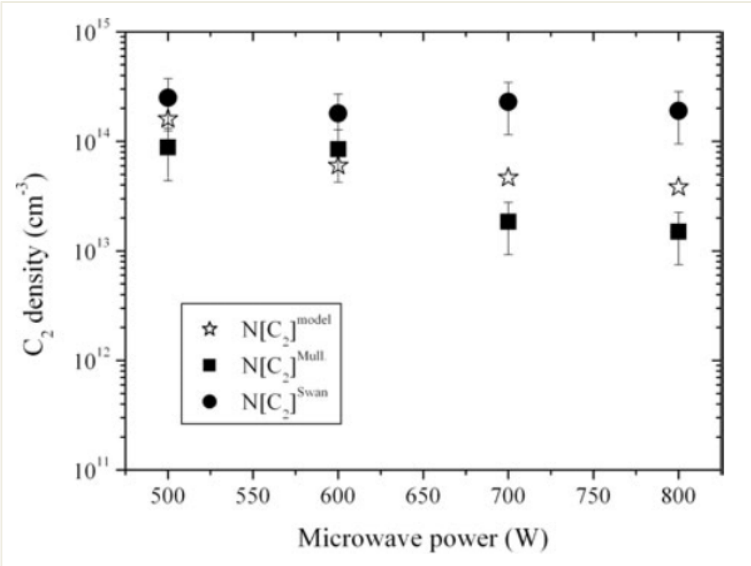


***$C_2$ absolute density** derived from BAS measurements ($C_2$ Mulliken and Swan systems).*
*$C_2$ density calculated with a 0D thermochemical plasma model*

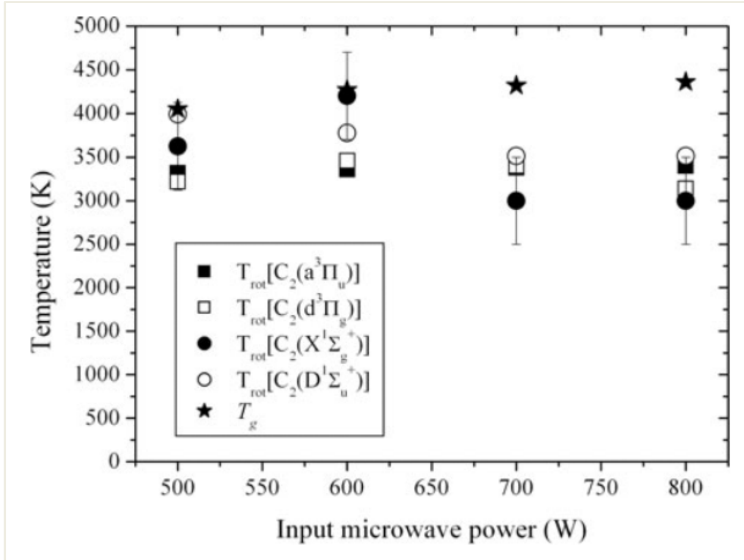


***Rotational temperatures** $T_{rot}(X^1\Sigma_g^+)$, $T_{rot}(D^1\Sigma_u^+)$, $T_{rot}(a^3\Pi_u)$ and $T_{rot}(d^3\Pi_g)$ determined by BAS and OES from $C_2$ Mulliken and Swan systems. Gas temperature $T_g$ calculated with a 0D thermochemical plasma model*

(*) G. Lombardi, K. Hassouni, F. Bénédic, F. Mohasseb, J. Röpcke, A. Gicquel, JAP 2004

# $H_2/CH_4/CO_2$ PLASMAS FOR LOW-TEMPERATURE NCD DEPOSITION

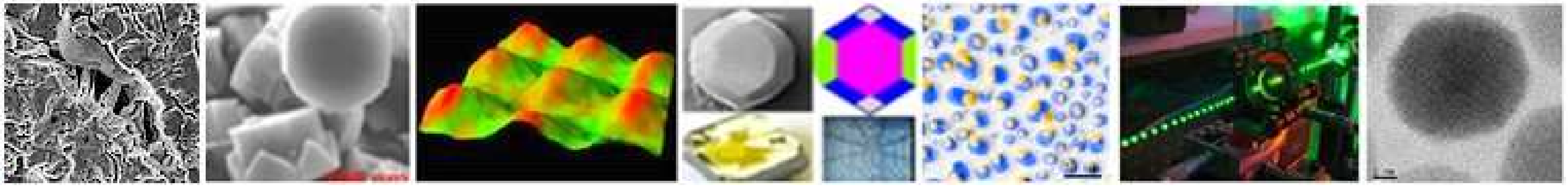



# $H_2/CH_4/CO_2$ plasmas for low temperature NCD deposition

**Limitations of NCD growth process:**

- Insufficient adhesion properties to substrates due to residual stress
- Damages on sensitive substrate because of high deposition temperature (above 800°C)

⇒ **Deposition of nano-crystalline diamond films at low-temperature needed**

**Plasmodie reactor**
**(PEMA team, 2010's)**

MW Power: 1-3 kW
$[H_2]$: 90-98 %
$[CH_4]$: 1-5 %
$[CO_2]$: 1-5 %
**Pressure: < 1 mbar**

**16 coaxial plasma sources** arranged in 4x4 2-D matrix

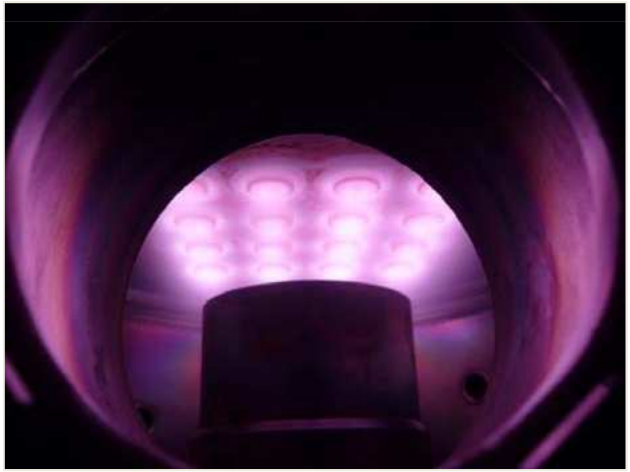

- Low substrate temperature: T < 500°C
- Large area deposition: 4 inches

**Some of the key parameters to control:**
**Gas temperature and CO kinetics (etching species, surface stabilizer)**

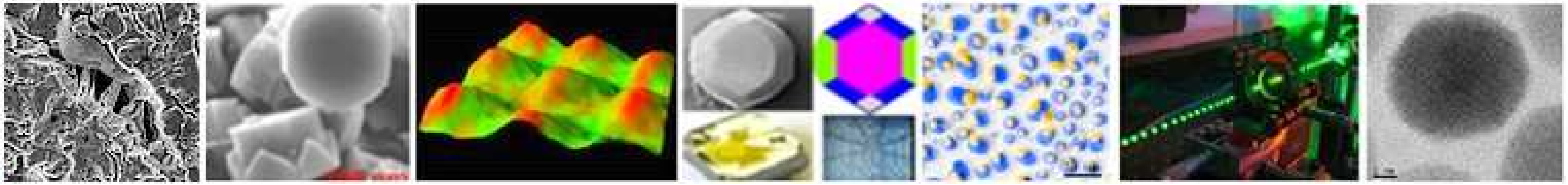

## $H_2/CH_4/CO_2$ plasmas for low temperature NCD deposition(*)

**Infrared absorption**

**External Cavity Quantum Cascade Laser**
→ **44 raies** CO lines of the 1st, 2nd and 3rd vibration excitation levels (100 $cm^{-1}$ scan)

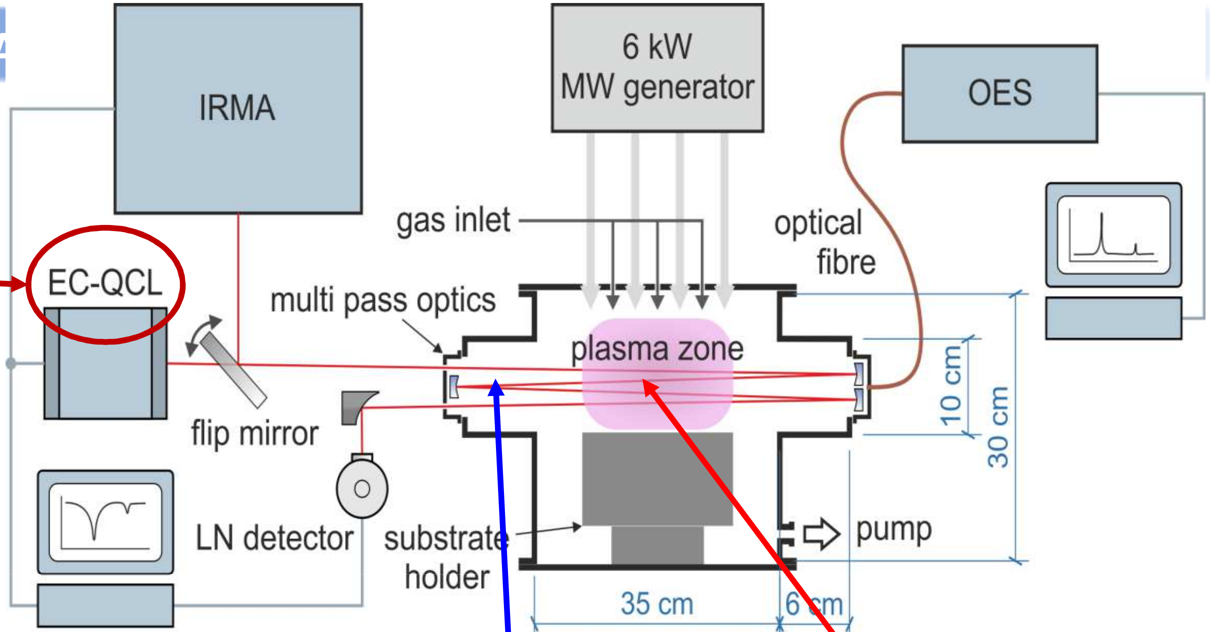


**Spatial information on gas temperature as a function of vibration excitation levels, despite integrated measurements**

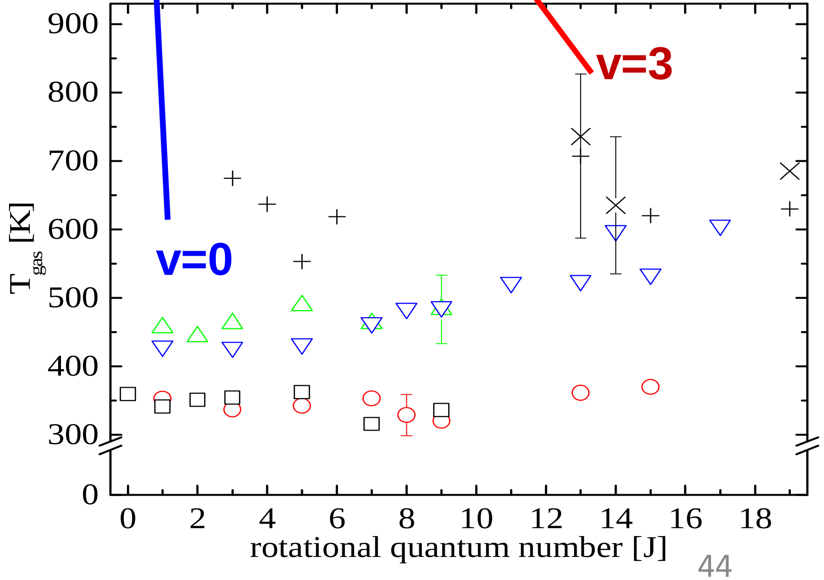


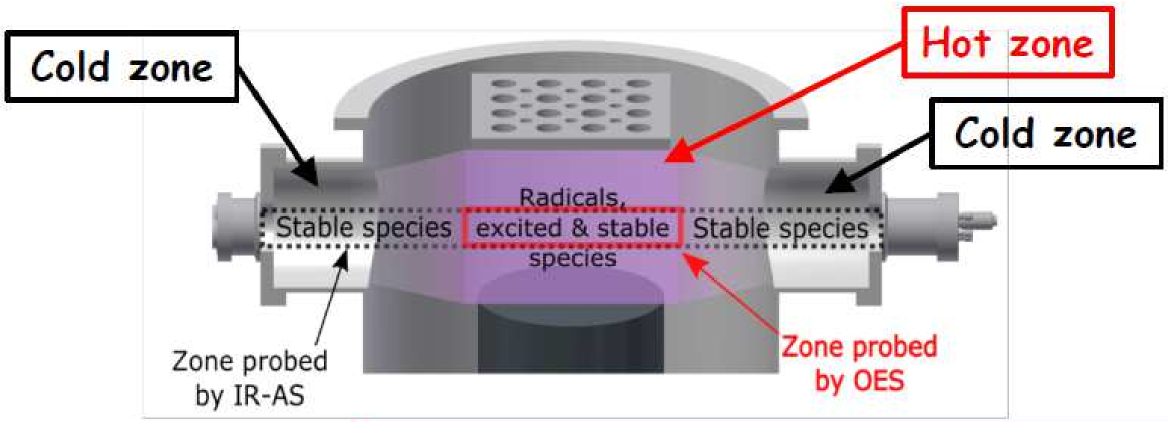




(*) A. Nave, B. Baudrillart, S. Hamann, F. Benedic, G. Lombardi, A. Gicquel, J. H. van Helden, J. Röpcke, PSST 2016 / PHC Procope 2015-2016

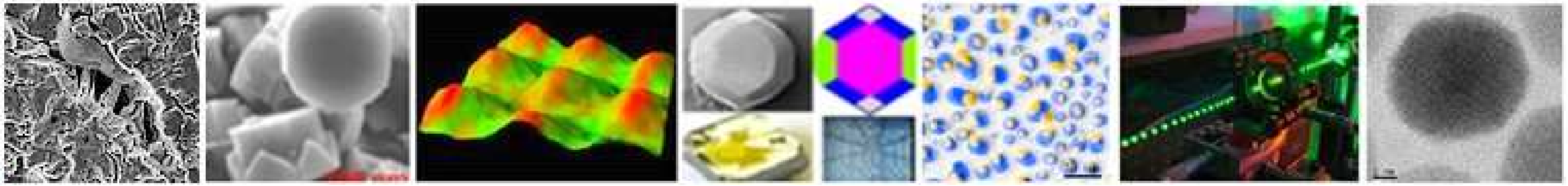



# Merci de votre attention !

# Et remerciements aux très nombreux contributeurs du LSPM:

J. Achard, X. Aubert, B. Baudrillart, O. Brinza, C. Duluard, A. Gicquel, K. Hassouni, R. Issaoui, G. Lombardi, A. Michau, S. Prasanna, C. Rond, F. Silva, A. Tallaire, M. Wartel

# XXX